

THE 2MASS WIDE-FIELD T DWARF SEARCH. IV. HUNTING OUT T DWARFS WITH METHANE IMAGING¹

C. G. TINNEY², ADAM J. BURGASSER^{3,6}, J. DAVY. KIRKPATRICK⁴, AND MICHAEL W. MCELWAIN⁵

(Received 2005 February 19; Accepted 2005 July 21)
To appear in The Astronomical Journal, Nov. 2005

ABSTRACT

We present first results from a major program of methane filter photometry for low-mass stars and brown dwarfs. The definition of a new methane filter photometric system is described. A recipe is provided for the differential calibration of methane imaging data using existing 2MASS photometry. We show that these filters are effective in discriminating T dwarfs from other types of stars, and demonstrate this with Anglo-Australian Telescope observations using the IRIS2 imager. Methane imaging data and proper motions are presented for ten T dwarfs identified as part of the 2MASS “Wide Field T Dwarf Search” – seven of them initially identified as T dwarfs using methane imaging. We also present near-infrared moderate resolution spectra for five T dwarfs, newly discovered by this technique. Spectral types obtained from these spectra are compared to those derived from both our methane filter observations, and spectral types derived by other observers. Finally, we suggest a range of future programs to which these filters are clearly well suited: the winnowing of T dwarf and Y dwarf candidate objects coming from the next generation of near-infrared sky surveys; the robust detection of candidate planetary-mass brown dwarfs in clusters; the detection of T dwarf companions to known L and T dwarfs via deep methane imaging; and the search for rotationally-modulated time-variable surface features on cool brown dwarfs.

Subject headings: infrared: stars – infrared: brown dwarfs – infrared: photometry

1. BACKGROUND

T dwarfs have the coldest photospheres (at least outside our Solar System) which are currently accessible to direct observation. With masses inferred to lie between $\sim 60 - 10M_{\text{JUP}}$, they represent a class of object linking the properties of observable low-mass stars and brown dwarfs, with the properties of unobservable extrasolar planets. The defining feature of these objects is the presence of strong, broad methane absorptions in the near-infrared at 1.3-1.4, 1.6-1.8 and 2.2-2.5 μm . When first seen in the prototype T dwarf Gl 229B (Nakajima et al. 1995), the distinctiveness of these spectroscopic features immediately suggested the need for a new spectral class. This “T” class was initially explored in two separate spectral typing schemes by Burgasser et al. (2002) and Geballe et al. (2002), which are in the process of being unified in to a single “hybrid” system (Burgasser et al. 2003a).

The methane features that define T dwarfs are so broad and distinctive, that the use of dedicated filters to detect them was a logical next step. Proof of concept observations of Gl 229B (Rosenthal et al. 1996) soon confirmed this expectation. Many more T dwarfs have been discovered in the years since, and there has been some additional exploratory work on the use of methane filters (Herbst et al. 1999; Mainzer & McLean 2003) using this larger sample of T dwarfs. Mainzer et al. (2004), in particular, have defined a four filter narrow-bandpass photometric system in the atmospheric H window (1.45-1.8 μm) designed for the detection and characterisa-

tion of young brown dwarfs in heavily reddened clusters. Golimowski et al. (2004) and Krist et al. (1998) have also presented results for methane imaging of nearby stars in a search for cool companions, based on a synthetic spectrum calibration. However, near-infrared J,H,K imaging and near-infrared spectroscopy remain the mainstay of T dwarf observational study. There has, as yet, been no large scale characterisation of observed T dwarfs using broad methane filters. Nor have methane filters yet been utilised where they are particularly powerful – as a quick and efficient way of characterising candidates arising from large photometric surveys as “T or non-T”, without the need for either photometric conditions or an infrared spectrograph.

We therefore set out to more fully explore the use of methane filters in the study of T dwarfs. Three steps were critical in this process: (a) defining a photometric calibration procedure for a new photometric system (denoted CH_{4s}, CH_{4l}, and CH_{4s}-CH_{4l}) using a set of broad methane filters with IRIS2 on the 3.9m Anglo-Australian Telescope (AAT); (b) exploring the use of Two Micron All Sky Survey (2MASS; Skutskie et al. 1997; Cutri et al. 2003) JHKs photometry to calibrate methane filter images differentially onto this CH_{4s}, CH_{4l}, CH_{4s}-CH_{4l} photometric system, and (c) using the resulting differential methane imaging to search for T dwarfs amongst the lists of candidates being identified in the 2MASS Wide-Field T Dwarf Search (WFTS) – a long-term program which has been conducting a search over 74% of the sky for T dwarfs in the 2MASS All-Sky database (Burgasser et al. 2003b,c, 2004a,b).

The selection criteria and selection procedures of the 2MASS WFTS are described in detail in Burgasser et al. (2003b). The most challenging aspect of this program is the extreme *rarity* of T dwarfs in a shallow magnitude-limited survey. The first-pass photometric selection criteria produce over a quarter of a million potential T dwarfs from the 1.3 billion sources in the 2MASS Point Source Catalogue. But our expectation is that this sample will only contain $\sim 20 - 30$

¹ Based on observations obtained at the Anglo-Australian Telescope, Siding Spring, Australia.

² Anglo-Australian Observatory, PO Box 296. Epping. 1710 Australia. cgt@aaoepp.aao.gov.au

³ Department of Astrophysics, American Museum of Natural History, New York NY 10024 USA. adam@amnh.org.

⁴ Infrared Processing & Analysis Center, Caltech, Pasadena, CA. 91125 USA. davy@ipac.caltech.edu

⁵ UCLA, 8371 Mathematical Sciences, CA. 90095. USA. mcelwain@astro.ucla.edu

⁶ Spitzer Fellow

actual T dwarfs. Visual examination of catalogue images are carried out on all the first pass candidates to eliminate $\sim 99.5\%$ of the faint background stars, proper-motion stars, closely separated visual binaries, and general chaff that contaminate the sample.

However, this still leaves ~ 1000 T dwarf candidates, which require further on-sky observations to winnow down to the much smaller number of actual T dwarfs expected. In the past, the procedure for doing this has been (Burgasser et al. 2002): near-infrared imaging to eliminate minor planets; followed by optical imaging to exclude background stars; followed by near-infrared spectroscopy to carry out final verification. The latter two steps are time consuming and expensive in telescope time, due to the faintness of these targets. Methane imaging offers the possibility of combining all three of these steps into one observation. A pair of 2-3 minute methane exposures on a 4m-class telescope can reveal; (a) whether there is still an infrared object present at the 2MASS position (i.e. eliminate uncatalogued minor planets); (b) the colour of the object in the methane filters (which can determine its ‘‘T or non-T’’ nature and estimate T spectral type); and (c) automatically provide proper motion data. Follow-up infrared spectroscopy, therefore, need only be carried out on a much smaller sample of high confidence T dwarf candidates, rather than the hundreds otherwise required. The greatly reduced data processing overhead of a pair of methane images, compared to infrared images, optical images and infrared spectroscopy, is also a significant advantage.

This is Paper IV in the series arising from the WFTS. Paper I (Burgasser et al. 2003b) describes the selection process for our T dwarf candidates in detail. Papers II-III (Burgasser et al. 2003c, 2004a) present initial T dwarf discoveries arising from the search. In this paper we describe the definition of a new CH_{4s}, CH_{4l}, CH_{4s}-CH_{4l} photometric system using methane filters, provide sequences relating infrared JHK colours to these methane colours, and describe a procedure for using 2MASS data to differentially calibrate observations onto that system. We present IRIS2 CH_{4s}-CH_{4l} data and proper motions for new T dwarfs identified by this program – five new T dwarfs, and a number of T dwarfs previously published by us (Burgasser et al. 2003c, 2004a), many of which were independently detected by our methane imaging in 2002-2003. In Section 3.1 we present spectra for a number of these new T dwarfs, obtained with the IRIS2 instrument, and demonstrate that these spectra confirm our methane filter detections. Finally, Section 4 discusses the extension of these techniques into other areas of T dwarf research.

2. METHANE IMAGING

2.1. Imaging with IRIS2

IRIS2 is an all-refracting 9 element focal-reducing collimator-camera, which is installed at the AAT’s $f/8$ Cassegrain focus. It provides a final f -ratio at its HAWAII1 HgCdTe detector of $f/2.2$, or a plate scale of $0.4486''$ per pixel. This results in a field-of-view $7.7'$ on a side. The optical train is capable of delivering 1 pixel full-width half-maximum images over the whole field of view. However, as with all focal reduction systems of this type, it introduces astrometric distortion into the detected images. IRIS2’s astrometric distortion is such that the plate scale in the corners of the detector is $\sim 1\%$ smaller than that at the field centre. It is quite precisely represented as a radial distortion, which can be parametrised by a quartic polynomial of the form

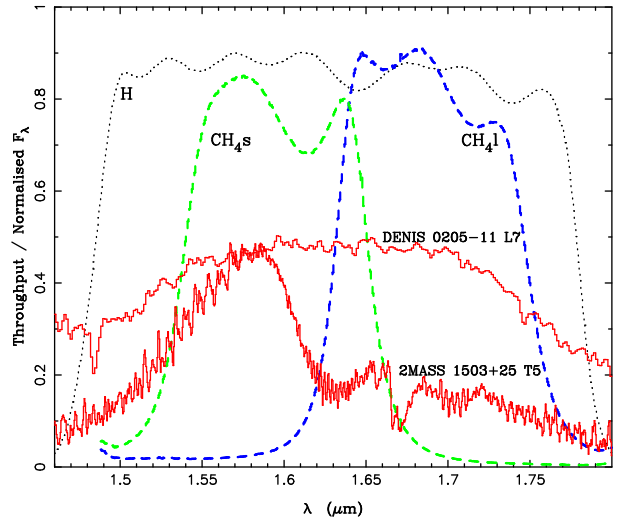


FIG. 1.— IRIS2 methane filters. The heavy dashed lines show the measured bandpasses of the IRIS2 CH_{4s} and CH_{4l} filters. The cut-on, central and cut-off wavelengths for the CH_{4s} and CH_{4l} filters are 1.520, 1.570, 1.620 μm and 1.640, 1.690, 1.740 μm (respectively). For comparison Mauna Kea Observatories H filter bandpass (also installed in IRIS2) is plotted as a dotted line. Spectra of the T5 dwarf 2MASS J15031961+2525196 (lower trace: SPEG data from Burgasser et al. (2004a)), and the L7 dwarf DENIS-P J0205.4-1159 (upper trace; CGS4 data from Leggett et al. (2001)). The two spectra have been normalised at $1.57\mu\text{m}$.

$$r = r'(1 - 2.4988 \times 10^{-6}r' - 4.4466 \times 10^{-11}r'^3) \quad (1)$$

where r' is the radius in observed pixels from a central pixel $(x_0, y_0) = (516.86, 515.02)$, and r is the radius in pixels from (x_0, y_0) in an ideal undistorted co-ordinate system with plate scale $0.4486''$ per pixel.⁷

IRIS2 contains a filter set acquired as part of one of the ‘‘Mauna Kea Observatories’’ infrared filter consortia. J,H,K and Ks filters were acquired from OCLI of Santa Rosa, CA in 1998, and a set of narrow- and intermediate-band filters were acquired from NDC Infrared Engineering, Essex, UK between 2000 and 2002. The J,H,K,Ks filters were manufactured to the ‘‘Mauna Kea Observatories Near-Infrared Filter Set’’ specifications of Tokunaga et al. (2002). The narrow- and intermediate-band set are as specified by A. Tokunaga⁸. In particular, the latter set includes a pair of methane filters, which we denote CH_{4s} and CH_{4l}, which are available in many other infrared instruments at telescopes around the world. Figure 1 shows the band-passes for these filters, superimposed on T and L dwarf spectra. The CH_{4l} filter samples the broad 1.6-1.8 μm methane absorption bands seen in T dwarfs, while the CH_{4s} filter samples pseudo-continuum outside the methane band – though as for all cool dwarf photospheres this pseudo-continuum is itself the result of significant molecular absorption – in this case largely H₂O.

2.2. IRIS2 Observations

Imaging observations in methane filters were acquired (in combination with a variety of other observing programs) on 29 nights in the period 2002 March 31 to 2004 March 9 with IRIS2. Observing conditions on these nights were highly variable – from good seeing in photometric conditions, to poor

⁷ See the IRIS2 web pages at <http://www.aaopt.gov.au/iris2/iris2.html> for details.

⁸ http://www.ifa.hawaii.edu/%7Etokunaga/NB_special_ordersort

seeing in partial cloud. (In many cases methane observations were carried out as a “poor conditions” backup to other observing programs.) Objects targeted for observation over the course of this program include known T dwarfs, known L dwarfs, a large number of candidate T dwarfs deriving from the 2MASS WFTS, and (in photometric conditions) UKIRT “Faint Standard” (FS) stars (Hawarden et al. 2001).

Observations with these filters are carried out by obtaining a series of dithered individual exposures in each filter. All these observations are performed under the control of an IRIS2 observing sequence, providing dithers in either fixed or pseudo-random patterns. As data is taken it is processed on-line using an implementation of the ORAC-DR data reduction pipeline⁹. ORAC-DR is a generic data reduction pipeline originally created at the Joint Astronomy Centre, Hawaii, for use with various UKIRT and JCMT instruments. It collects sets of observations of a target in a single filter into a *group*. It generates a first pass flat-field for the *group* by suitably normalising and creating a median image. It uses these first-pass flattened data to detect objects, mask them out, and flag bad pixels. It then creates a final flat field by taking the median of this normalised and masked data, and applies it to the raw data to create a *flattened group*. The flattened group images are re-sampled to remove astrometric distortion, objects are re-detected and offsets between images estimated using these detections. The images are then re-sampled again onto a uniform co-ordinate system to create a single *final* image. All of this processing is carried out on a dedicated data-reduction 3.3Ghz Linux PC, resulting in fully processed images within 30s of an observing sequence completing – usually before the telescope has even been moved to the next observing target.

2.3. A Methane Photometric System

To calibrate the methane colours of T dwarfs, extensive observations of both UKIRT FS stars, and known M, L and T dwarfs were obtained on at least three photometric nights over the course of our observing program: 2002 October 21; 2003 January 25; and 2004 March 1. There are no pre-existing photometric standards for use with such filters, so we elected to define our own photometric system based on the Mauna Kea Observatories (MKO) H-band photometry of UKIRT FS stars¹⁰. Additional JHK photometry on the same MKO system for a number of M, L and T dwarfs was obtained from Leggett et al. (2002) and Knapp et al. (2004). Where MKO JHK photometry for M, L and T dwarfs observed in the methane filters was not available, we converted 2MASS All Sky photometry (Cutri et al. 2003) to the MKO system using published spectral types, and the conversion functions of Stephens & Leggett (2004).

Aperture photometry was measured for all the targets observed on these nights. For bright targets, large photometric apertures (10-15'' in radius) were chosen, resulting in <0.005 magnitudes in flux being missed outside the aperture. For fainter targets, photometry was performed in smaller (2-4'' radius apertures), and bright objects in the same image were used to determine aperture corrections to the same large apertures as used for brighter objects. Uncertainties due to the standard-error-in-the-mean of these aperture corrections (estimated on an image-by-image basis) and the <0.005 mag. flux potentially missed outside the outer aperture, were carried through all subsequent calculations.

TABLE 1
CH₄S AND CH₄L PHOTOMETRIC PARAMETERS

Night	Airmass Correction, A^a		Zero-point, ZP	
	CH ₄ s	CH ₄ l	CH ₄ s	CH ₄ l
2002 October 21	0.03±0.03	0.03±0.03	10.46±0.03	10.46±0.02
2003 January 25	0.03±0.03	0.03±0.03	10.76±0.02	10.76±0.02
2004 March 1	0.42±0.01	0.45±0.01	10.35±0.06	10.35±0.06

^a Calibrated magnitude = $-2.5\log_{10}(counts/t_{exp}) - A \times airmass + 31 - ZP$.

We adopted UKIRT FS stars of spectral types A, F and G as fundamental standards. This spectral type range was chosen because (as we show below) it shows essentially zero CH₄s–CH₄l colour variation. We assign to these UKIRT FS stars magnitudes in the CH₄s and CH₄l filters identical to their MKO H magnitudes, and from this determine photometric calibrations (both airmass corrections and zero-points) on each night. These are reported in Table 1. In all but one case, the CH₄s and CH₄l airmass corrections and zero-points were consistent with being the same (on a given night), so average values were adopted and are reported in the table. The exception was 2004 March 1, where the airmass corrections were not consistent with a single value, and so different values were used. Both airmass corrections on this night were also significantly larger than those obtained on the other two nights, and the photometric zero-point has significantly larger uncertainties. This night was warm, humid and somewhat hazy, which is thought to be the reason for the larger extinction and poorer photometric accuracy. There is also significant variation from night-to-night in the photometric zero-point. These variations most likely reflect the fact these filters sample the edges of the atmospheric water vapour absorption bands which define the H window (at least at the Siding Spring site). Night-to-night variations in the amount of water vapour absorption will result in differing zero-points. However, since the critical parameter these filters measure is the *difference* between CH₄s and CH₄l, so long as observations in the two filters are closely spaced in time and airmass, these variations are essentially irrelevant.

2.4. Methane Photometry

2.4.1. CH₄s–CH₄l and Spectral Type

These observations therefore provide photometry in CH₄s, CH₄l and, most importantly, CH₄s–CH₄l colour. Figure 2 shows CH₄s–CH₄l colour as a function of spectral type. Spectral type is parametrised numerically as n , such that for A to T type stars n is the spectral subtype plus a constant : 0 for an A dwarf; 10 for F; 20 for G; 29 for K; 35 for M; 45 for L and 54 for T. While it was not our intention in this study to study the detailed methane spectroscopy of white dwarfs, nonetheless three UKIRT FS white dwarfs were observed during the course of this program, which we have put at the “placeholder” position of $n = -1$. The objects plotted (and tabulated in Table 7) are: UKIRT FS stars with spectral types A-K stars from Hawarden et al. (2001) and for white dwarfs from McCook & Sion (1999); M dwarfs with Leggett et al. (2002) spectral types; L dwarfs with Kirkpatrick et al. (2000) types, except for 2M1045-0149 (Gizis 2002) and DEN1539-0520, which is based on a Keck optical spectrum analysed so as to place it on the Kirkpatrick et al. (2000) system (D. Kirkpatrick, private communication); and T dwarfs with spectral types on a variant of the hybrid T typing scheme which was

⁹ <http://www.oracdr.org/>

¹⁰ <http://www.jach.hawaii.edu/UKIRT/astronomy/calib/phototypes>

preliminarily proposed by Burgasser et al. (2003a), but modified to use slightly different indices and spectroscopic reference standards as described in Section 3.2. Table 7 also provides the average $\text{CH}_4\text{s}-\text{CH}_4\text{l}$ colours for all the objects in Figure 2, along with the spectral types and JHK colours adopted, so that others using such filters can calibrate their data onto a uniform system.

As suggested above, the variation in $\text{CH}_4\text{s}-\text{CH}_4\text{l}$ colour across the A, F and G spectral types is negligibly small, which is why these stars were chosen to define the photometric system. K, M and L dwarfs have slightly positive $\text{CH}_4\text{s}-\text{CH}_4\text{l}$ colours (i.e. they are red in these filters), while T dwarfs show a marked trend to become bluer with increasing T spectral type. Figure 2 also shows a parametrisation for this relationship, as follows,

$$\text{CH}_4\text{s}-\text{CH}_4\text{l} = n(0.0087 + 6.176 \times 10^{-6} n^2 + 1.202 \times 10^{-9} n^4 - \frac{0.519}{68.5 - n}) \quad (2)$$

While this function is numerically valid to $n < 68.5$, it is only constrained by data in the range $0 < n < 62$ (i.e. the white dwarfs do not constrain the fit). Root-mean-square (rms) scatter about this fit is 0.07 mag over the whole spectral type range. More critically the rms scatter is 0.11 mag for T dwarfs and 0.04 mag for L0-T2 dwarfs.

2.4.2. $\text{CH}_4\text{s}-\text{CH}_4\text{l}$ and JHK colours

While the relationship between $\text{CH}_4\text{s}-\text{CH}_4\text{l}$ colour is useful for assigning T spectral types, it is not the only tool for examining the potential T dwarfs in large photometric surveys like 2MASS or the forthcoming UKIRT Infrared Deep Sky Survey (UKIDSS¹¹ Hambly et al. (2003)). These surveys will also produce JHK photometry, providing additional data on whether or not a given object is likely to be a T dwarf.

Figure 3 shows plots of $\text{CH}_4\text{s}-\text{CH}_4\text{l}$ colour as a function of J-H, H-K and J-K colour (on the MKO photometric system) for the objects (except the white dwarfs) presented in Figure 2. The JHK photometry for these objects comes from (in order of preference): the UKIRT MKO photometric standards database¹⁰; from Leggett et al. (2002); from Knapp et al. (2004); or by converting 2MASS All Sky data into the MKO system using the conversion relations of Stephens & Leggett (2004). Clearly the dwarf sequence has a complex behaviour in these diagrams, with the added complication of significant scatter among the T dwarfs.

To try and clarify this behaviour we have combined the $\text{CH}_4\text{s}-\text{CH}_4\text{l}$ versus spectral type relations derived above, with JHK versus spectral type sequences for dwarf stars. The latter have been derived using the spectral types of Hawarden et al. (2001) for UKIRT MKO photometric standards, supplemented by published M, L and T types (see Sections 2.4.1 and 3.2 for details and references) for a number of cool dwarfs with existing MKO JHK photometry (Leggett et al. 2002; Knapp et al. 2004). The resulting sequences are shown in Figure 5. Tests with polynomials of both low and high order show that these curves are not readily amenable to simple parametrisation, so we have parametrised the J-K and H-K sequences by binning the available data in spectral type (large open squares in the figure), and interpolating a cubic-spline through these data points (solid line in the figure).

These near-infrared sequences, combined with the $\text{CH}_4\text{s}-\text{CH}_4\text{l}$ versus spectral type sequences derived above, produce “tracks” in the $\text{CH}_4\text{s}-\text{CH}_4\text{l}$ versus colour planes, which are shown in Figure 3. These tracks tell us (among other things) that to discriminate between early T dwarfs and the M-L dwarfs, $\text{CH}_4\text{s}-\text{CH}_4\text{l}$ photometry must be sufficiently precise to reveal the 0.2 mag gap between these two classes of object. The sequences are tabulated in Table 2.

One notable feature of these tracks is the inflection at $J-H \approx 0.5$ in the J-H versus $\text{CH}_4\text{s}-\text{CH}_4\text{l}$ plane, which is simply the mapping into J-H versus $\text{CH}_4\text{s}-\text{CH}_4\text{l}$, of the well known inflection in the J-H versus H-K diagram, which is produced as giants bifurcate from dwarfs at mid-M spectral types (see for example Bessell & Brett (1988), Figure A3).

2.5. Differential Methane Photometry

While photometry is essential to underpin our determination of the relationship between near-infrared colour, spectral type and $\text{CH}_4\text{s}-\text{CH}_4\text{l}$ colour, the observational overheads in obtaining such data are large, leading us to ask “Can we make do with differential photometry?”. Since both our bands can be observed nearly simultaneously, at identical airmasses in similar seeing and transparency conditions, systematic uncertainties in aperture corrections due to seeing variations, extinction corrections due to airmass variations, and (to some extent) zero-point corrections due to transparency variations, can all be cancelled out. The availability of the 2MASS All Sky data provides an additional incentive to the differential approach, since H-band calibration photometry is available over almost 100% of the sky.

Our $\text{CH}_4\text{s}-\text{CH}_4\text{l}$ photometric system is defined based on MKO H photometry for standard stars of spectral type A, F and G. Or equivalently in colour space $-0.021 < (J-K)_{\text{MKO}} < 0.456$, $-0.021 < (H-K)_{\text{MKO}} < 0.086$, or $0.00 < (J-H)_{\text{MKO}} < 0.370$. To use 2MASS photometry to calibrate the same data, we can transform these colour ranges into the appropriate 2MASS ranges using the conversions provided by the 2MASS All-Sky Survey Explanatory Supplement¹² for A-M dwarfs, supplemented by the conversions of Stephens & Leggett (2004) for L-T dwarfs. Figure 4 shows the $\text{CH}_4\text{s}-\text{CH}_4\text{l}$ versus $(J-H)_{\text{MKO}}$ relation derived above, along with the comparable $\text{CH}_4\text{s}-\text{CH}_4\text{l}$ versus $(J-H)_{2\text{MASS}}$ relation obtained by transforming MKO colours to 2MASS colours. (J-H has been chosen for this plot as it is the colour most commonly available for objects in the 2MASS All Sky catalogue – similar relations have been derived for the other JHK colours). In principle, therefore, one could select background stars in a pair of $\text{CH}_4\text{s}, \text{CH}_4\text{l}$ frames with 2MASS colours corresponding to A-G spectral types – $-0.023 < (J-K)_{2\text{MASS}} < 0.472$, $-0.002 < (H-K)_{2\text{MASS}} < 0.091$, or $-0.038 < (J-H)_{2\text{MASS}} < 0.390$. Unfortunately, even with a field of view as large as that of IRIS2 (7.7' on a side), this often restricts the number of objects available for calculating a zero point to less than 2 per field.

However, Fig. 4 indicates that a much larger range of colours could be used to calculate a zero-point, if one was able to parametrise the variation in $\text{CH}_4\text{s}-\text{CH}_4\text{l}$ as a function of 2MASS colour. The solid lines in Figure 4 represent a parametrisation for $(J-H)_{2\text{MASS}}$ which has been adopted to do this. We avoid the region $0.5 < (J-H)_{2\text{MASS}} < 0.6$ where the sequence is degenerate, and fit two separate quadratics to the

¹¹ <http://www.ukidss.org/>

¹² <http://www.ipac.caltech.edu/2mass/releases/allsky/doc/sec6>

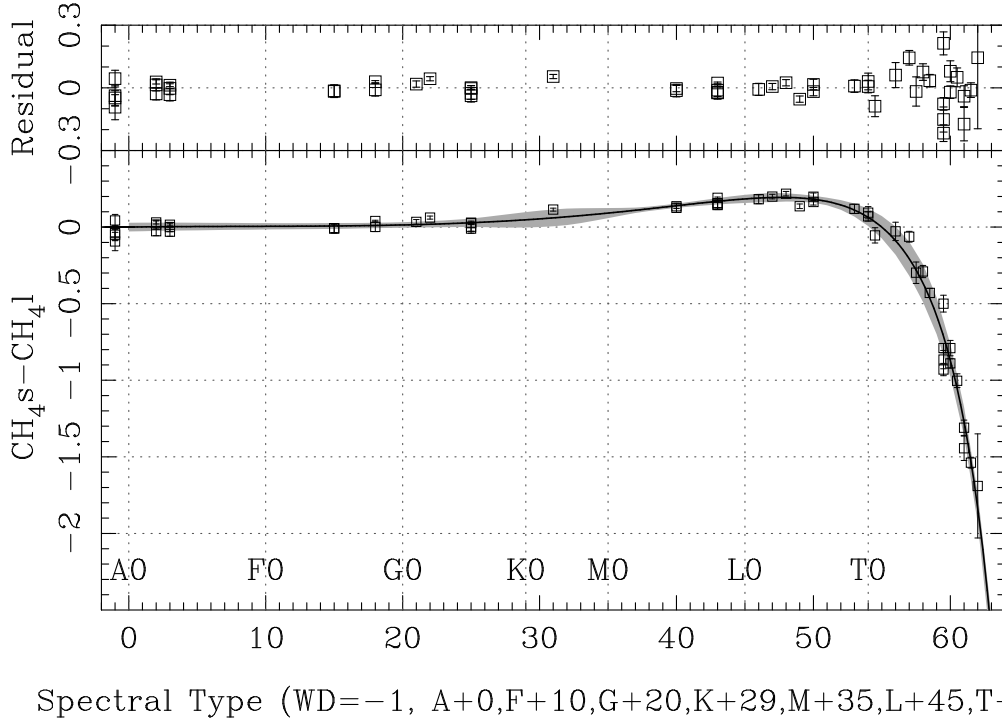


FIG. 2.— IRIS2 methane colour ($\text{CH}_4\text{s}-\text{CH}_4\text{l}$) as a function of A-T spectral type. The uncertainties plotted are the combination of photon-counting uncertainties, aperture correction uncertainties and photometric calibration uncertainties. Typical uncertainties on spectral types (not plotted) are ± 0.5 . See the text for references to the spectral type sources and for the form of the plotted parametrisation. Root-mean-square (rms) scatter about the parametrisation (grey shading) is 0.07 mag for the whole range, 0.04 mag for L0-T2 dwarfs and 0.11 mag for T dwarfs.

TABLE 2
SPECTRAL TYPE, METHANE AND JHK COLOUR SEQUENCES

SpT	$\text{CH}_4\text{s}-\text{CH}_4\text{l}^{\text{a}}$	MKO			2MASS		
		J-H ^b	H-K ^b	J-K ^b	J-H ^c	H-K ^c	J-K ^c
A0	+0.000	+0.000	-0.021	-0.021	-0.038	-0.002	-0.023
A5	+0.004	+0.087	+0.006	+0.093	+0.063	+0.021	+0.095
F0	+0.005	+0.146	+0.027	+0.173	+0.131	+0.039	+0.178
F5	+0.007	+0.214	+0.032	+0.246	+0.209	+0.044	+0.254
G0	+0.014	+0.225	+0.040	+0.265	+0.222	+0.051	+0.274
G5	+0.028	+0.288	+0.075	+0.363	+0.295	+0.081	+0.375
K0	+0.047	+0.407	+0.092	+0.499	+0.432	+0.096	+0.516
K3	+0.067	+0.504	+0.110	+0.614	+0.545	+0.112	+0.636
M0	+0.091	+0.519	+0.174	+0.693	+0.562	+0.167	+0.718
M2	+0.110	+0.495	+0.252	+0.747	+0.534	+0.235	+0.774
M4	+0.129	+0.486	+0.340	+0.826	+0.524	+0.311	+0.856
M6	+0.149	+0.512	+0.426	+0.938	+0.554	+0.386	+0.972
M8	+0.168	+0.595	+0.495	+1.090	+0.650	+0.446	+1.129
L0	+0.184	+0.698	+0.568	+1.266	+0.853	+0.538	+1.391
L2	+0.193	+0.792	+0.651	+1.443	+0.958	+0.579	+1.537
L4	+0.190	+0.878	+0.723	+1.601	+1.056	+0.633	+1.689
L6	+0.167	+0.981	+0.794	+1.775	+1.173	+0.706	+1.879
L8	+0.111	+1.009	+0.756	+1.765	+1.218	+0.685	+1.903
T0	+0.064	+0.956	+0.673	+1.629	+1.176	+0.615	+1.791
T1	-0.001	+0.810	+0.532	+1.342	+1.041	+0.490	+1.531
T2	-0.089	+0.517	+0.281	+0.798	+0.761	+0.257	+1.018
T3	-0.207	+0.211	+0.055	+0.266	+0.470	+0.050	+0.520
T4	-0.365	-0.006	-0.051	-0.057	+0.269	-0.036	+0.233
T5	-0.579	-0.126	-0.047	-0.173	+0.167	-0.012	+0.156
T6	-0.870	-0.225	-0.045	-0.270	+0.088	+0.011	+0.099
T7	-1.270	-0.340	-0.083	-0.423	-0.004	-0.007	-0.012
T8	-1.834	-0.460	-0.137	-0.597	-0.100	-0.042	-0.142

^aSequence represented by equation 2.

^bSpline sequences as shown in Fig 5.

^cMKO sequences converted to 2MASS system as described in the text.

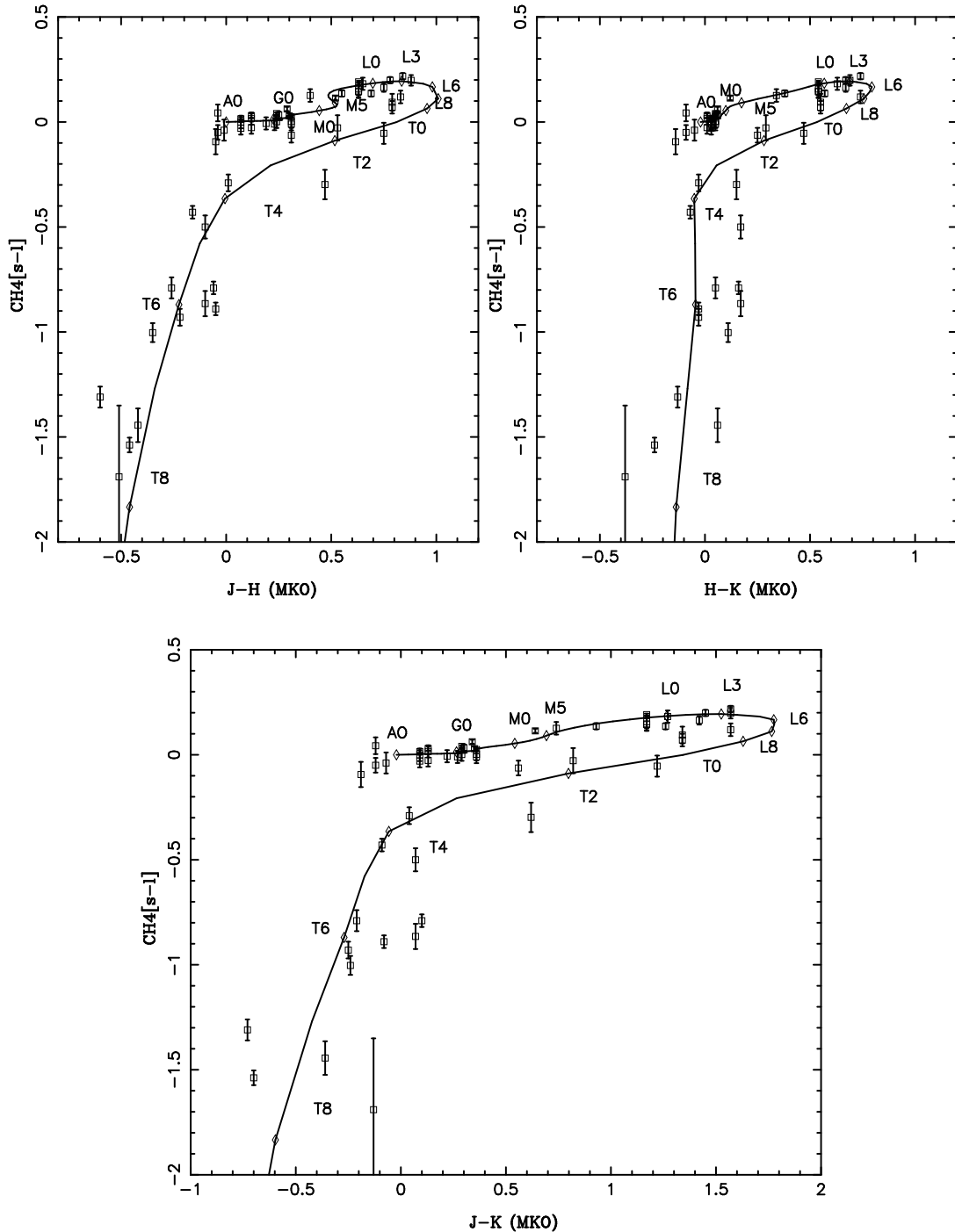


FIG. 3.— IRIS2 methane colour ($CH_{4s}-CH_{4l}$) as a function of J-H, H-K, and J-K (MKO) colour. The $CH_{4s}-CH_{4l}$ uncertainties plotted are the combination of photon-counting uncertainties, aperture correction uncertainties and photometric calibration uncertainties. JHK photometry and uncertainties are from UKIRT WWW pages, MKO photometry from Leggett et al. (2002) or 2MASS photometry converted to the MKO system using the conversion relations of Stephens & Leggett (2004). The overplotted tracks and spectral types (*solid lines and open diamonds*) are produced from the $CH_{4s}-CH_{4l}$ versus spectral type relation of Fig. 2, and the JHK-colour versus spectral type relations of Fig. 5 and Table 2. Note the four white dwarf observations which when plotted in this plane, lie just to the left of the A0 end of the plotted sequence.

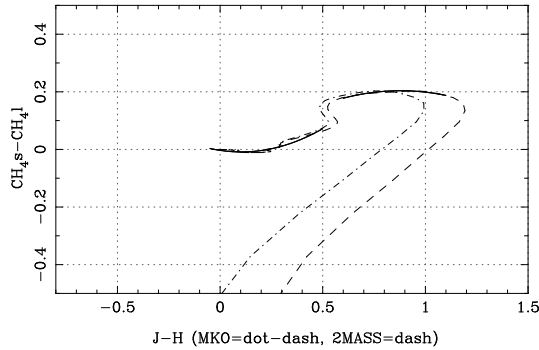


FIG. 4.— $\text{CH}_4\text{s}-\text{CH}_4\text{l}$ dwarf sequence as a function of $J-H$ in the MKO and 2MASS systems. MKO curve (*dot-dashed line*) comes from the parametrisations in Fig. 3 and 2MASS (*dashed line*) curve is the MKO curve transformed using the conversions in the 2MASS Explanatory Supplement and Stephens & Leggett (2004). The solid lines are polynomial fits to ranges $(J-H)_{\text{MKO}} = -0.05-0.5$ and $0.6-1.1$ which are non-degenerate and useful for determining the $\text{CH}_4\text{s}-\text{CH}_4\text{l}$ zero point of observations with 2MASS photometry.

regions $-0.05 < (J-H)_{2\text{MASS}} < 0.5$,

$$\text{CH}_4\text{s} - \text{CH}_4\text{l} = -0.0015 - 0.0.00864(J-H) + 0.2569263(J-H)^2 \quad (3)$$

and $0.6 < (J-H)_{2\text{MASS}} < 1.1$,

$$\text{CH}_4\text{s} - \text{CH}_4\text{l} = -0.0378 + 0.47851(J-H) - 0.249901(J-H)^2. \quad (4)$$

Of course, these relations are also degenerate with the T dwarf branch of the sequence. We therefore adopt a two-stage calibration approach – by rejecting from the second pass any objects within $10''$ of any known or suspected T dwarfs in the field, and any objects with $\text{CH}_4\text{s}-\text{CH}_4\text{l} < -0.2$, we eliminate any T dwarfs which might contaminate this calibration.

The following procedure, therefore, enables the use of the ensemble of background stars in a field-of-view to derive a robust differential $\text{CH}_4\text{s}-\text{CH}_4\text{l}$ in even non-photometric conditions :

1. Select and photometer stars in CH_4s and CH_4l images. We carried out this step using the Starlink implementation of SExtractor¹³ (Bertin & Arnouts 1996). It is important to note that the detailed parameters used in this process are not critical, since the only aim is to obtain robust *relative* photometry for all the objects in a field of view.
2. Obtain 2MASS JHK photometry in the field of view – these can be downloaded from the GATOR server at IRSA¹⁴.
3. Match the CH_4s , CH_4l and 2MASS objects. Our implementation of this step was carried out using Michael Richmond’s *match* code¹⁵.
4. Avoiding any known or suspected T dwarfs within the field of view, select matched objects with $-0.05 < (J-H)_{2\text{MASS}} < 0.5$ and $0.6 < (J-H)_{2\text{MASS}} < 1.1$ and uncertainty in 2MASS magnitude less than 0.1 mag. Then use

¹³ <http://terapix.iap.fr/soft/sextractor/index.html>

¹⁴ <http://irsa.ipac.caltech.edu/applications/Gator/>

¹⁵ <http://spiff.rit.edu/match/>

equations 2 and 3 to estimate the $\text{CH}_4\text{s}-\text{CH}_4\text{l}$ for these objects based on their $J-H$ colour, and derive a first pass zero-point $\text{CH}_4\text{s}-\text{CH}_4\text{l}$ calibration.

5. Repeat this step, further rejecting any objects with $\text{CH}_4\text{s}-\text{CH}_4\text{l} < -0.2$ from the first pass.
6. Apply this zero-point calibration to place data on the $\text{CH}_4\text{s}-\text{CH}_4\text{l}$ system.

We have found that a typical IRIS2 field of view will contain between 5 and 15 suitable background objects, leading to zero point calibrations with a standard error in the mean of < 0.05 mag.

Figure 6 shows a plot of the photometry (used to define our methane photometric system in Section 2.3) versus differential methane photometry calculated for the same observations using the procedure above. The dotted line shows the one-to-one relationship between the two sets of measurements, while the solid line is a least squares fit between the two, with the following form

$$(\text{CH}_4\text{s} - \text{CH}_4\text{l})_{\text{Diff}} = 0.029 \pm 0.001 + (1.006 \pm 0.004)(\text{CH}_4\text{s} - \text{CH}_4\text{l}) \quad (5)$$

The rms scatter in differential $\text{CH}_4\text{s}-\text{CH}_4\text{l}$ about this fit is 0.05 mag. These results indicate that differential $\text{CH}_4\text{s}-\text{CH}_4\text{l}$ photometry can be used with confidence at the 0.05 mag level.

2.6. Methane Imaging Results

With a typical methane imaging observation consisting of 3-5 dithered observations in each of the methane filters, and exposure times of 30-60 s, a complete WFTS candidate sequence takes ~ 5 minutes to complete. The ORAC-DR system is able to process these data to publication standard on the fly, and a perl script automates the processing described in the previous sections, allowing nearly on-line analysis of each observation during each night (or at the very latest, on the following afternoon). This has the advantage of allowing almost immediate IRIS2 spectroscopic follow-up of T dwarfs identified by our methane imaging.

To date, we have observed 508 candidate T dwarfs identified as part of the WFTS – of these 61 revealed no infrared counterpart to the original 2MASS detection, while the remainder were detected in the CH_4s and CH_4l bands. Of these detected objects: 10 have $\text{CH}_4\text{s}-\text{CH}_4\text{l}$ colours indicating they are T dwarfs, and have been spectroscopically confirmed as T dwarfs; 2 have colours suggesting they may be T dwarfs, and have been ruled out by spectroscopy; and 3 objects have $\text{CH}_4\text{s}-\text{CH}_4\text{l}$ colours suggesting they may be early T dwarfs and are awaiting spectroscopy to confirm their status. Of the 10 T dwarfs detected by methane imaging from the WFTS, seven (2M0034-33, 2M1122-35, 2M1114-26, 2M0939-24, 2M0949-15, 2M1828-48, 2M2331-47) were first confirmed as T dwarfs by methane imaging, while a further three were imaged in methane filters after their spectra had been acquired elsewhere (Burgasser et al. 2003c, 2004a). Finding charts for all of these T dwarfs are shown in Figure 7.

Figure 8 summarises the results of these differential methane observations. It plots $\text{CH}_4\text{s}-\text{CH}_4\text{l}_{\text{Diff}}$ against 2MASS $J-H$ for (1) a sample of known T and L dwarfs; (2) the T dwarfs identified from the WFTS; (3) objects detected by the WFTS methane imaging, but not T dwarfs; (4) a few objects whose methane photometry is not decisive and which need additional spectroscopy to clarify their status; and (5) underlying these data is the “haze” of background objects observed

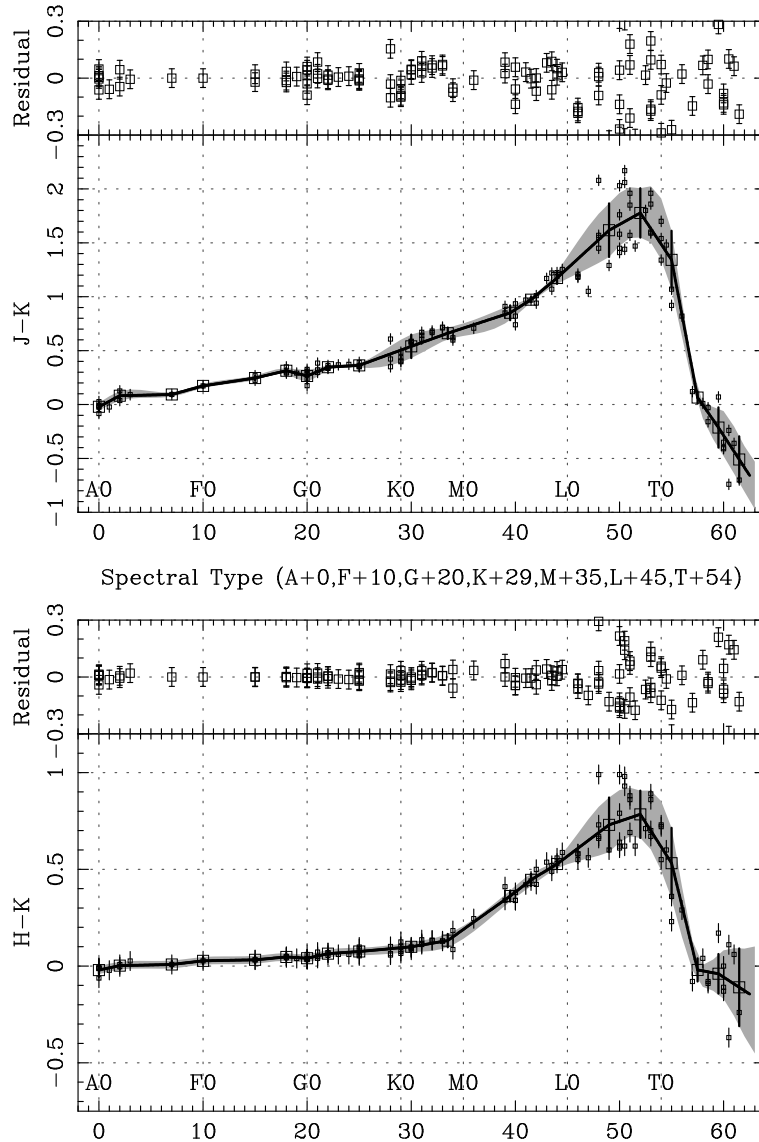


FIG. 5.— J-K and H-K (MKO) as a function of A-T spectral type. JHK photometry and uncertainties are from UKIRT WWW pages, and MKO photometry from Leggett et al. (2002) for M, L and T dwarfs (*small squares*). These data have been binned by spectral type (*large squares*), which have themselves been fitted with a cubic-spline interpolating function (*solid line*). The shaded region shows the $1\text{-}\sigma$ rms scatter about the binning. These tracks are summarised in Table 2.

in these 508 IRIS2 observations with 2MASS photometric uncertainties < 0.05 mag, and within $3'$ of the IRIS2 field centre. The $\text{CH}_4\text{s}-\text{CH}_4\text{l}$ versus $(\text{J}-\text{H})_{2\text{MASS}}$ sequence of Table 2 is also plotted. The T dwarf differential photometry from this figure is also summarised in Table 8.

These results reinforce the power of methane imaging – we have reduced the need for spectroscopic confirmation, from hundreds of objects to fifteen. It should be noted, however, that while the methane imaging technique is quite clean for late T dwarfs (of the seven WFTS candidates imaged in methane and found to have $\text{CH}_4\text{s}-\text{CH}_4\text{l} < -0.5$, all are spectroscopically found to be T dwarfs), it becomes progressively less so for early T dwarfs (both the “ruled out by spectroscopy” methane candidates have $\text{CH}_4\text{s}-\text{CH}_4\text{l} > -0.3$). For early T dwarfs the large number of background objects with neutral $\text{CH}_4\text{s}-\text{CH}_4\text{l}$ colours, leads to photometric and differential zero-point uncertainties scattering increasing numbers of background objects into regions where their colours mimic

those of early T dwarfs. Similarly, the rate at which T dwarfs could be “missed” by our methane imaging is a strong function of spectral type. As Table 7 indicates, we easily re-detect based on $\text{CH}_4\text{s}-\text{CH}_4\text{l}$ colour alone, all eleven known T dwarfs later than T4, while for types earlier than T2 position information in addition to $\text{CH}_4\text{s}-\text{CH}_4\text{l}$ colour is necessary to identify the T dwarf. A detailed analysis of all the WFTS candidates observed (required to examine the efficiency of methane imaging as a function of spectral type, and so produce selection functions and luminosity functions from our survey) is postponed to a subsequent paper when the entire WFTS results will be presented and analysed.

A notable feature of Fig. 8 is that the bluest objects in J-H lie systematically below the $\text{CH}_4\text{s}-\text{CH}_4\text{l}-(\text{J}-\text{H})_{2\text{MASS}}$ sequence. This is an artefact of the initial colour criteria adopted for selection from 2MASS, the 0.1-0.2 mag uncertainties on these colours, and the relative numbers of intrinsically red and blue stars in the 2MASS database. Figure 1 of Burgasser et al.

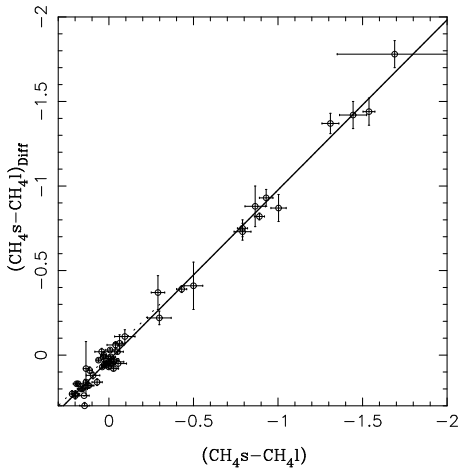


FIG. 6.— $(\text{CH}_4\text{s}-\text{CH}_4\text{l})$ measurements plotted against $(\text{CH}_4\text{s}-\text{CH}_4\text{l})_{\text{Diff}}$ measurements obtained from the same data frames. The dotted line is the one-to-one relationship, while the solid line is the least squares fit described in the text. The scatter in $(\text{CH}_4\text{s}-\text{CH}_4\text{l})_{\text{Diff}}$ about the fit is 0.05 mag.

(2003c) shows how the selection used by the WFTS leads to peaks in the number of objects selected at $(\text{J}-\text{H})_{2\text{MASS}} \approx 0.7$ (equivalent to mid- to late-M dwarfs) and $(\text{J}-\text{H})_{2\text{MASS}} \approx 0.3$ (equivalent to early- to mid-G dwarfs). However, M dwarfs hugely outweigh G dwarfs in the 2MASS database, meaning that photometric uncertainties scatter many more actual M dwarfs into the G dwarf “peak” than there are real G dwarfs in that peak. This is reflected in Fig. 8 where we see that most of the objects in the G dwarf “peak” at $(\text{J}-\text{H})_{2\text{MASS}} \approx 0.3$ have $\text{CH}_4\text{s}-\text{CH}_4\text{l}$ colour appropriate for M dwarfs, not G dwarfs.

Proper motions have been estimated for all the T dwarfs listed in Table 8. These were calculated by: projecting the 2MASS data in each field into a tangent plane centred on the 2MASS target catalogue coordinate; using the `match`¹⁵ code to determine a linear transformation for each astrometrically corrected IRIS2 image to this tangent plane; and estimating the motion between the observation epoch in the 2MASS catalogue and the IRIS2 observation epoch. Typical astrometric uncertainties due to this process are in the range 0.1-0.2”, and typical epoch differences are 4-5 yr. Many of the T dwarfs listed in Table 8 will be at distances of 7-20 pc, and so will have annual parallax motions of 0.125-0.05”, which we have not attempted to control. These will introduce proper motion uncertainties of a magnitude similar to those due to the precision of the astrometric transformation between the two epochs.

3. SPECTROSCOPY

3.1. IRIS2 Spectroscopy

Spectroscopic observations were carried out with IRIS2 on the nights of 2003 July 12-14, 2004 January 8 and 2004 March 3-9 (UT). The targets observed are summarised in Table 3. Observations were obtained with a 1” slit (corresponding to 2.2 pixels on the detector) in one of three configurations.

J1 : (Jlong) a 240 line/mm transmission grating bonded to a sapphire prism (“Sapphire240”) used in the collimated beam of IRIS2, together with a spectroscopic blocking filter denoted “J1” (which transmits $\lambda=1100$ -1350 nm) to deliver 0.232 nm per pixel spectra over the wavelength range 1105.2-1343.4 nm on the detector, with a resolution of 2.3 pixels, corresponding to

$$\lambda/\Delta\lambda = R \approx 2290 - 2250.$$

Hs : (Hspect) a 316 line/mm transmission grating bonded to a sapphire prism (“Sapphire316”) used with a spectroscopic blocking filter denoted “Hs” (which transmits $\lambda=1443$ -1824 nm) to deliver 0.346 nm per pixel spectra over the wavelength range 1485-1795 nm (this wavelength range being primarily determined by terrestrial water vapour transmission), with a resolution of 2.3 pixels, corresponding to $\lambda/\Delta\lambda = R \approx 2050 - 2150$.

H : the same configuration as Hs, but with the MKO H filter used as a spectroscopic blocker. In this mode, the filter bandpass ($\lambda=1485$ -1795 nm) sets the spectral format recorded (which is nonetheless very similar to that delivered by Hs).

Wavelength calibrations were obtained with a Xe lamp, which enables a third-order polynomial dispersion fit to be obtained with rms scatter about the fit of better than 1/20th of a pixel.

The spectra were acquired by nodding the telescope between two beams (“A” and “B”) in either AB or ABBA combinations, with observations at each beam of 300s-600s. For spectroscopic observing the detector was operated in Multiple Read Mode (MRM), with typically 60 non-destructive reads being acquired over the course of the exposure, and the final image being obtained from a least-squares fit to each pixel. This mode delivers an effective read noise in the final image of less than 5 electrons.

Data reduction followed a more-or-less standard procedure for infrared spectrographs. The first step for all images was to create a Poisson uncertainty image based on the known gain, read-noise and dark current of IRIS2. The astrometric distortion present in IRIS2 images (see above), delivers spectra with significant curvature (i.e. arc and sky lines are curved on the IRIS2 focal plane). For each spectroscopic configuration, arc lines were used to construct a correction which removes this curvature using the Figaro `sdist` and `cdist` codes. These were applied to flat-field images (obtained by subtracting images of the AAT dome obtained when illuminated with a quartz-halogen lamp, from images obtained with the lamp turned off) to produce a “straightened” flat field image. The spectral response of this flat-field was then determined by collapsing this image in the spatial direction, and making a smooth spline fit through it. By then growing this smooth spectral response into an image, and reversing the distortion correction, we obtained an image which could normalise the raw flat-field images, and provide a true “pixel-to-pixel” spectroscopic flat-field.

All images were flattened with these flat fields, and then sky subtracted with the relevant exposures in the AB or ABBA observing pattern. The IRIS2 astrometric distortion was then removed, delivering spectra with constant wavelength at all columns on the detector, with the majority of the sky lines subtracted (though changes in the strength of the near-infrared night sky lines always result in some residual differences being present in these sky-subtracted images). The tilt of the dispersed spectra relative to the detector rows ($<0.5^\circ$) was then removed.

The observed targets were identified in these processed images, and used to define windows for a further sky subtraction pass (by fitting along the columns of the detector), followed by flagging of cosmic rays by hand, and then optimal extraction. At each step of this process, the initial photon-counting errors are propagated, so that the final result is a

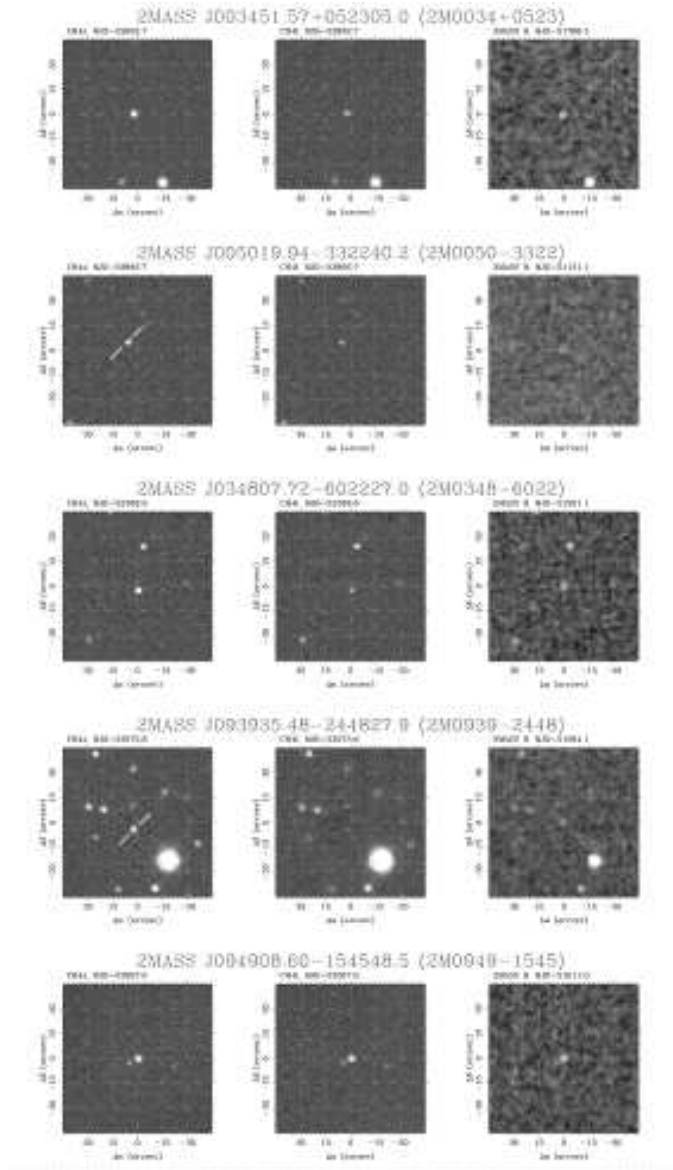


FIG. 7.— Finding charts for WFTS objects listed in Table 8. For each object, images 3' on a side, centred on the 2MASS Point Source Catalog (PSC) position indicated, in CH₄s, CH₄l and 2MASS H are shown. Epochs are indicated by their Modified Julian Dates. Also shown superimposed on the H-band charts are all the 2MASS PSC sources in each field of view. The WFTS T dwarfs are highlighted in the methane images where proper motions make identification unclear.

spectra with meaningful uncertainties. Wavelength calibration was obtained by passing Xe arc lamp images through the same process, and extracting them from the same detector regions as each object.

The same procedures were used to reduce observations of A, F and G stars obtained either immediately before, or immediately after our target star, in the same instrument configurations. These were used to correct the effects of terrestrial atmospheric absorption for each target, assuming a blackbody flux distribution for each terrestrial correction star based on their spectral type. The strong hydrogen absorption lines in the H-band spectra of A type stars were found to make them essentially useless for this purpose, so these spectra were discarded. These terrestrial correction stars not only enable us to remove the effects of atmospheric absorption, but also to place our final spectra on a meaningful F_{λ} flux scale – though with arbitrary zero-point calibration uncertainty due to the slit losses when observing the terrestrial calibration star.

For purposes of spectral typing, the main features of interest are broad, so we have binned our spectra from their full $R \approx 2200$ resolution to $R \approx 370$ (i.e. binned by a factor of 6). The binning weighted each pixel by the inverse square of its uncertainty, resulting in pixels lying on strong night sky lines receiving low weight in the final binning – effectively “software night sky suppression”. Tests with our spectra show that this procedure can deliver spectra with a given signal-to-noise ratio with an efficiency about 1.4-1.7 times faster than is possible by simply observing at $R \approx 370$.

3.2. Analysis

To place our spectra in a spectral typing sequence (and to derive uniform types for all the T-dwarfs observed in our methane filters), we numerically quantify the large-scale appearance of these using near-infrared spectroscopic indices. Numerous authors (following on from the initial work of Jones et al. 1994, 1996) have shown that near-infrared spectra

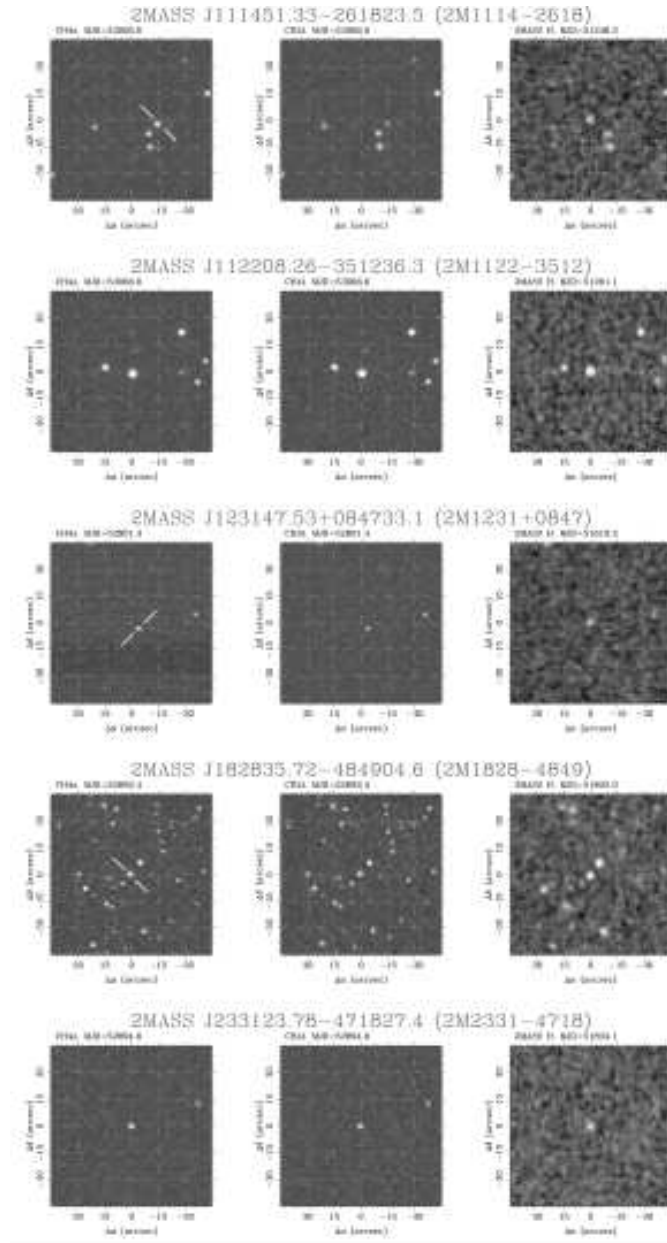


FIG. 7.— (continued)

TABLE 3
IRIS2 SPECTROSCOPIC OBSERVING

Night	Object	Formats ^a	Exposures (s)	Seeing ($''$)
2004 Jan 08	2M0050-3322	Jl,H	4×600s,4×600s	1.5
2004 Jan 08	SD0423-0114	Jl,H	4×300s,4×300s	1.9
2004 Jan 08	2M0559-1404	Jl,H	4×300s,4×300s	2.0
2004 Mar 03	2M1114-2618	Jl,Hs	4×600s,4×600s	2.4
2004 Mar 04	2M1122-3512	Jl,Hs	4×300s,4×300s	1.9
2004 Mar 04	2M1114-2618	Jl,Hs	4×300s,4×300s	1.7
2004 Mar 08	2M0949-1545	Jl,Hs	2×600s,2×600s	2.4
2004 Mar 09	2M0939-2448	Hs	2×600s	2.2

^a See Section 3.1 for wavelength coverage and resolutions of these formats

offer multiple features which can be used to classify ultra-cool dwarfs. The use of near-infrared spectroscopic indices to quantify the strength of broad molecular features in ultra-cool dwarfs was pioneered by Delfosse et al. (1997) (see also Tinney et al. 1998; Delfosse et al. 1999), and has since been extended throughout the M and L spectral types by Reid et al. (2001), who used the optical M and L dwarf spectral classification system of Kirkpatrick et al. (2000) as their fundamental standards, and derived calibrations to transfer infrared spectral indices onto these optical L types. Testi et al. (2001) have continued in this vein for a sample of L dwarfs observed in the near infrared at very low resolution. For T dwarfs, near-infrared spectra *define* the spectral type. Two separate infrared typing schemes were initially developed by Burgasser et al. (2002) and Geballe et al. (2002) (the latter including additionally a near-infrared classification of L dwarfs). Both

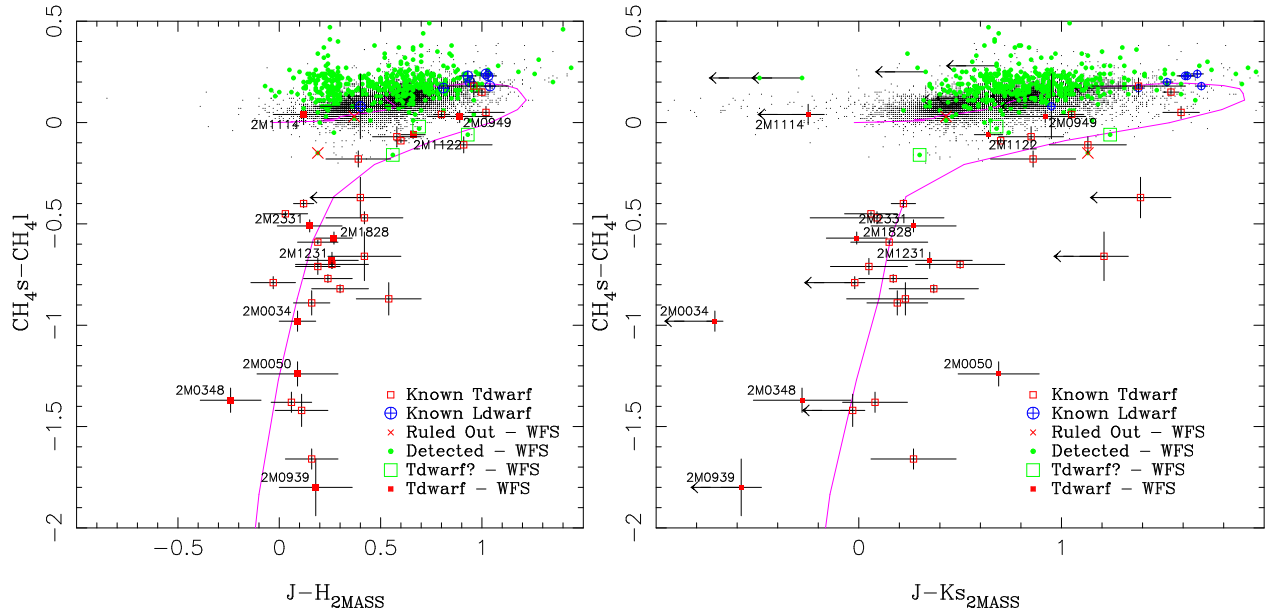


FIG. 8.— $(\text{CH}_4\text{s}-\text{CH}_4\text{l})_{\text{Diff}}$ plotted against 2MASS J-H and J-Ks for Wide Field T dwarf Search (WFTS) candidates observed to date. Objects not detected at Ks or H by 2MASS are indicated as colours with upper limits. WFTS T dwarfs are plotted as solid squares with labels. WFTS objects which were detected, but not indicated as being T dwarfs by their $\text{CH}_4\text{s}-\text{CH}_4\text{l}$ photometry, are plotted as solid circles, and objects whose $\text{CH}_4\text{s}-\text{CH}_4\text{l}$ photometry suggests a T dwarf status (but not yet confirmed by spectra) are highlighted with large open squares, while those where spectra have ruled out a T dwarf status are over plotted with diagonal crosses. Known T dwarfs are shown as open squares (where more than one observation has been taken, they are an average), and known L dwarfs as open circles with crosses. The haze of small points underlying the plot shows all background objects observed during this program, within $3'$ of the centre of the IRIS2 field-of-view, and with 2MASS uncertainties of <0.05 mag.

are based on spectroscopic indices which are sensitive to the strength of H_2O and CH_4 molecular absorption. A “hybrid” scheme was proposed by Burgasser et al. (2003a) to bring these two schemes into alignment. Preliminary spectral indices and spectroscopic standards for this hybrid scheme were presented by Burgasser et al. (2004a); the final version of this scheme is imminent (Burgasser et al. 2005).

To classify the T dwarfs identified by methane-band imaging, we used the H_2O^I , CH_4^I , H_2O^H , and CH_4^H indices of Burgasser et al. (2005). (These are the same as those in Burgasser et al. 2004a, but with the numerator of the CH_4^I index shifted redward by $0.015\mu\text{m}$.) We have used publicly available L dwarf (Knapp et al. 2004)¹⁶ and T dwarf¹⁷ spectra to calibrate these indices (Table 4). These are monotonic in the H_2O indices for L and T dwarfs, and monotonic in the CH_4 indices for objects later than L6. They therefore enable a spectral type to be estimated from each index for each T dwarf, with the final spectral type being adopted as the mean of these values (rounded to the nearest half sub-type).

These indices and the derived spectral types are summarised in Table 5 for the T dwarfs observed with IRIS2. The uncertainties listed on these types are the standard error in the mean. These types were then used to “order” our spectra in a sequence with comparison spectra – both our spectra (thick lines) and comparison spectra (underlying thin lines) are shown in Figure 10 – each segment of IRIS2 spectrum being normalised to the comparison spectrum on which it is plotted. The spectra classifications derived are consistent between the H- and J-band spectra for all the new T dwarfs, except for 2M0949-1545 and 2M1122-3512. For these objects the spectral type indicated by the H-band spectra are somewhat later than those indicated by the J-band spec-

TABLE 4
SPECTROSCOPIC COMPARISON OBJECTS

SpT	Object
L0	2MASS J03454316+2540233
L0.5	2MASS J07464256+2000321
L3	DENIS-P J1058.7-1548, 2MASS J15074769-1627386
L3.5	2MASS J00361617+1821104
L4.5	2MASS J00283943+1501418, 2MASS J22244381-0158521
L5	DENIS-P J1228.2-1547AB
L6.5	2MASS J22443167+2043433
L7	DENIS-P J0205.4-1159
L7.5	2MASS J08251968+2115521
L8	2MASS J03105986+1648155, 2MASS J03284265+2302051
L8	2MASS J15232263+3014562, 2MASS J16322911+1904407
T0	SDSSp J042348.57-041403.5
T1	SDSSp J015141.69+124429.6
T2	SDSSp J125453.90-012247.4
T3	2MASS J12095613-1004008
T4	2MASS J22541892+3123498
T5	2MASS J15031961+2525196
T6	SDSSp J162414.37+002915.6
T7	2MASS J07271824+1710012
T8	2MASS J04151954-0935066

NOTE. — Adopted types from Kirkpatrick et al. (2000) for L dwarfs and Burgasser et al. (2005) for T dwarfs.

tra. This could be due to the effects of unresolved binarity, or to an underlying structure in the CH_4^H index calibration, which is not adequately parametrised by the polynomial fits shown in Fig. 9. In either case, the spectral types for these objects should be regarded as somewhat more uncertain than for the other T dwarfs presented.

¹⁶ <http://www.jach.hawaii.edu/%7Esk1/LTdata.html>

¹⁷ <http://research.amnh.org/%7Eadam/tdwarf>

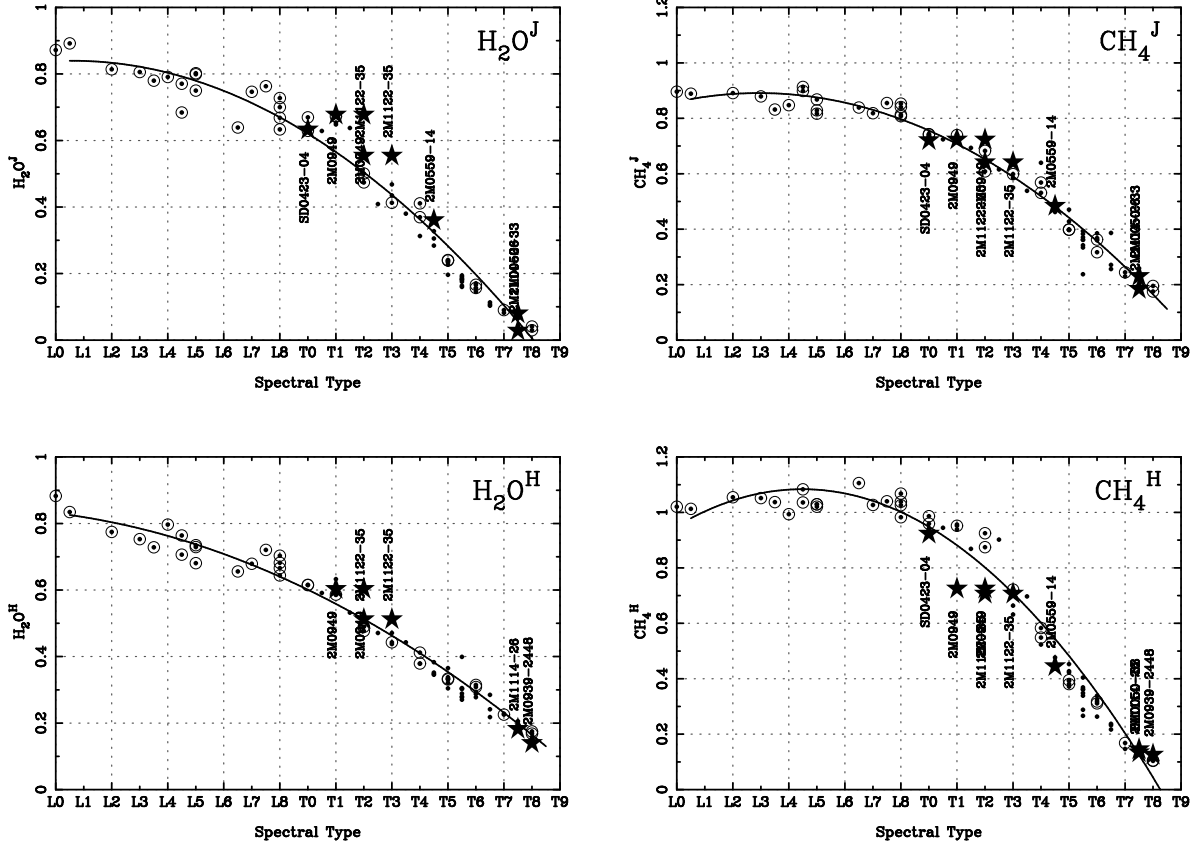


FIG. 9.— Spectroscopic classification indices for both our fundamental calibration objects (circles with solid dots), other known T dwarfs with “hybrid” T types (solid dots), and objects observed with IRIS2 (stars).

TABLE 5
SPECTROSCOPIC SPECTRAL TYPING RESULTS.

Object	H_2O^J	CH_4^J	H_2O^H	CH_4^H	$\langle SpT_{spec} \rangle$	SpT_{hyb}	$\langle SpT_{CH_4} \rangle$
SD0423-0114	0.63 ± 0.04	0.93 ± 0.03		0.92 ± 0.05	$T0.5 \pm 1.0$	T0	L3-T0
2M0949-1545	0.68 ± 0.04	0.94 ± 0.03	0.60 ± 0.03	0.72 ± 0.05	$T1.0 \pm 1.0$		$T0.3 \pm 1.5$
2M1122-3512	0.55 ± 0.04	0.89 ± 0.04	0.51 ± 0.03	0.71 ± 0.05	$T2.0 \pm 0.5$		$T1.5 \pm 1.1$
2M0559-1404	0.36 ± 0.04	0.79 ± 0.04		0.44 ± 0.05	$T4.5 \pm 0.5$	T4.5	$T4.1 \pm 0.4$
2M0050-3322	0.08 ± 0.04	0.46 ± 0.04		0.14 ± 0.05	$T7.5 \pm 0.5$		$T7.1 \pm 0.3$
2M1114-2618	0.03 ± 0.04	0.38 ± 0.04	0.18 ± 0.03	0.13 ± 0.05	$T7.5 \pm 0.5$		$T7.5 \pm 0.3$
2M0939-2448			0.14 ± 0.03	0.13 ± 0.05	$T8.0 \pm 0.5$		$T8.2 \pm 0.3$

TABLE 6
DISTANCE AND TANGENTIAL VELOCITY ESTIMATES FOR WFTS T DWARFS

Object Name	SpT^a	2MASS J	$d(\text{pc})^b$	$V_{tan}(\text{km s}^{-1})^c$
2M0034+0523	T6.5	15.54±0.04	9	37±19
2M0050-3322	T7.5	15.93±0.07	8	55±13
2M0348-6022	T7	15.32±0.05	7	24±6
2M0939-2448	T8	15.98±0.10	8	46±8
2M0949-1545	T1	16.15±0.12	20	10±6
2M1114-2618	T7.5	15.86±0.08	7	109±20
2M1122-3512	T2	15.02±0.04	14	19±5
2M1231+0847	T5.5	15.57±0.07	15	114±24
2M1828-4849	T5.5	15.18±0.05	12	21±7
2M2331-4718	T5	15.66±0.07	18	18±9

NOTE. — *a* - Spectroscopic spectral type from Table 5 (where IRIS2 spectra are available) and Table 8 otherwise. *b* - Distance estimate using 2MASS J absolute magnitude versus spectral type relation of Tinney et al. (2003) resulting in typical distances uncertainties of $\pm 20\%$. *c* - Uncertainty includes 0.36 mag scatter about absolute magnitude spectral type relation and photometric uncertainties for each T dwarf.

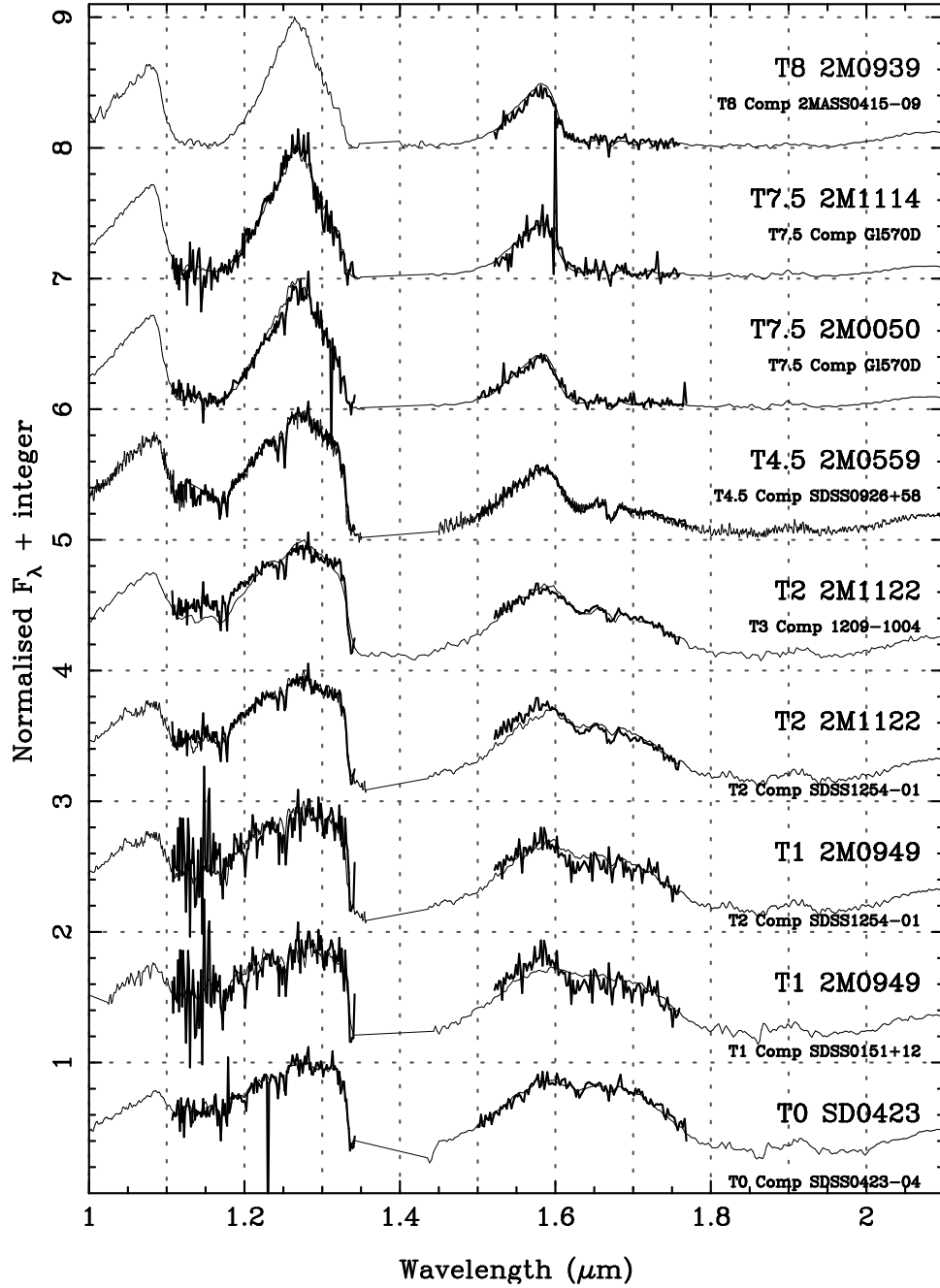


FIG. 10.— IRIS2 T dwarf spectra (thick lines) overlaid on T dwarf comparison spectra (thin lines – see Section 3.2). The spectral types assigned to the IRIS2 spectra are from Table 5. The adopted comparison spectral types are from the final hybrid classification scheme of Burgasser et al. (2005).

4. DISCUSSION

4.1. *The New T dwarfs*

Five of the WFTS T dwarfs reported in Table 8 (2M0050-3322, 2M0939-2448, 2M0949-1545, 2M1114-2618 & 2M1122-3512) are reported for the first time by this paper. A further four objects (2M0034+0523, 2M1231+0847, 2M1828-4849 & 2M2331-4718) were confirmed as T dwarfs by our methane imaging in parallel with the traditional spectroscopic approach, and have already been published by Burgasser et al. (2004a,b). Three of the five new T dwarfs (2M0050-3322, 2M1114-2618 & 2M0939-2448) are very cool objects with spectral types of T7.5 or later. In comparison, the other two objects are very early – at T1 (2M0949-1545) and T2 (2M1122-3512) they are the earliest T dwarfs yet found by selection for T dwarfs from the 2MASS database.

Of the WFTS T dwarfs reported here, 2M0939-2448 shows pronounced evidence in Fig. 8 for the same K-suppressed spectrum previously seen in 2M0034+0523 (Burgasser et al. 2004a) and 2M0937+2931 (Burgasser et al. 2002) – both 2M0939-2448 and 2M0034+0523 stand out as having the bluest J-Ks colours of any of the T dwarfs plotted (and indeed being only upper limits at Ks in 2MASS). Their J-H colours, by contrast are not anomalous in any way whatsoever. Note that the anomalously red J-Ks colours of SD0207+0000 and SD1110+0116 are not physical, but reflect the upper limits for K-band detection from 2MASS of these faint SDSS-discovered objects. On the other hand 2M0050-3322 does seem to be anomalously red for its methane index. A detailed discussion of the possible causes of K-band flux suppression in T dwarfs is postponed to a forthcoming paper.

Spectro-photometric distance estimates have been derived using the 2MASS J absolute magnitude versus spectral type relation of Tinney et al. (2003). These result in typical distances uncertainties of $\pm 20\%$ and are presented in Table 6. They place all of these WFTS T dwarfs at distances of between 5 and 20 pc, making them all likely members of the important and well studied “Nearby Star” volume-limited sample of objects within 25 pc of the Sun. They are all ideal targets for a 4m-class telescope near-infrared parallax program, and we initiated such a program with IRIS2 on the AAT in 2004. Of these T dwarfs, two (2M1114-2618 and 2M1231+0847) show appreciable proper motions, indicating tangential velocities $\gtrsim 100 \text{ km s}^{-1}$.

4.2. *Applications of Methane Imaging*

As outlined in section 1, methane imaging offers significant advantages over current techniques for the identification and classification of T dwarfs. We have shown this is particularly true for “winnowing” these rare objects from a large database like 2MASS, where we could use methane imaging in place of the combination of infrared imaging plus optical imaging plus infrared spectroscopy previously employed. Moreover, the greatly simplified data processing allows almost instantaneous feed back and spectroscopic confirmation, if necessary.

4.2.1. *Large Survey Winnowing*

Perhaps the most obvious application for methane imaging is the winnowing of forthcoming large surveys for cool brown dwarfs. The UKIRT Infrared Deep Sky Survey (UKIDSS; Hambly et al. 2003), for example, will carry out surveys in the Y, J, H and K passbands totalling a volume sensitivity for cool brown dwarfs almost 250 times larger than that obtained

by 2MASS. While the filters used in these surveys will be far more suitable for the selection of cool brown dwarfs than those used by 2MASS (Leggett et al. 2005), it is nonetheless true that T dwarfs in UKIDSS will represent a similar, tiny fraction of the total number of sources ($\lesssim 3 \times 10^{-5}$) as was seen in 2MASS. Hard won experience shows that when selecting objects this rare from a large database, the resulting sample is *always* dominated by contaminants – detector artefacts, ghosts, asteroids, cosmic rays, partially resolved binaries, confused sources near the survey limits, etc. Such contaminants produce catalogue sources with arbitrarily odd colours, some of which will mimic T dwarfs. The class of brown dwarfs cooler than T dwarfs (tentatively known as the “Y” dwarfs, and one of the key science drivers for the UKIDSS survey) will be even rarer, and candidate samples will be subject to even more contamination. Models for these objects suggest that they will have extremely unusual colours, and will lie some way from the sequence of foreground and background G-M dwarfs in a J-H versus Y-J colour-colour diagram – as much as a magnitude redder in Y-J, and a magnitude bluer in J-H. The ± 0.1 - 0.2 mag photometric uncertainties of objects near the survey magnitude limits will only rarely scatter G-M dwarfs by the 5- 10σ needed to move such objects into the Y dwarf selection region. But this will only need to happen at a rate of once in a billion to still massively outnumber the likely number of true Y dwarfs in the survey.

Some form of winnowing of candidates is almost inevitably going to be required before taking $H \approx 18$ Y dwarf candidates to an 8m telescope for infrared spectroscopy. Methane imaging offers an ideal mechanism for doing this, since $H \approx 18$ can be imaged on a 4m telescope in under an hour, compared to the several hours required to acquire spectra on an 8m telescope.

4.2.2. *Cluster T dwarfs*

It has been a common-place amongst astronomers for many years that there must exist a minimum mass for star formation, below which the mass function “turns over”. Based initially on Jeans mass arguments (Low & Lynden-Bell 1976), and later on hydrodynamic simulations (Boss 1988, 1993) this minimum mass was placed at $\sim 0.01 M_{\odot}$ (or $\sim 10 M_{\text{JUP}}$). The similarity of this value with the minimum mass for deuterium burning at $\sim 13 M_{\text{JUP}}$, has led to a 10- $13 M_{\text{JUP}}$ value being widely assumed as the minimum mass for star formation (or the maximum mass for planet formation¹⁸) and so as a dividing line between stars and planets. Below this mass, compact astrophysical objects are assumed to form *within* planetary disks via the “bottom up” processes of planetary accretion. Unfortunately, this comforting paradigm has become somewhat more confused of late.

1. Boss (2001) has included some magnetic field effects in simulations which show that star formation processes can make compact objects as small as $1 M_{\text{JUP}}$.
2. Candidate objects with masses which theoretical models suggest have masses similar to and smaller than $10 M_{\text{JUP}}$, are being turned up by surveys in star forming regions, in an apparent extension of “star” formation to “planetary” masses. These potentially “unbound” planets represent a challenge and a conundrum for the simple paradigm above – are they brown dwarfs formed via

¹⁸ <http://www.ciw.edu/boss/IAU/div3/wgesp/definition.html>

star formation processes, stellar embryos ejected from multiple systems before they can accrete sufficient matter to become stars (Reipurth & Clarke 2001), or giant planets ejected from their host stars?

3. Measurements of the brown dwarf mass function in a variety of moderate age clusters (>100 Myr) are finding results in the range $\propto m^{-0.5}$ to $\propto m^{-0.6}$ (Bouvier et al. 2003) suggesting a mass function which is continuous with the stellar function, but which continues to turn over at lower and lower masses, extending into the T dwarf range in some clusters.
4. Radial velocity programs are now detecting more massive analogues (extending up to $15 M_{\text{JUP}}$) of the $m \sin i = 0.1\text{--}5 M_{\text{JUP}}$ exoplanets. The mass function of these exoplanets is consistent with a single power law $\propto [m \sin i]^{-0.8}$ or steeper (Marcy et al. 2004). This is *steeper* again than the cluster brown dwarf mass function.

There is a need to clarify the status of the mass function in the range where the lines between planets and brown dwarfs are so blurred. Determining the relative normalisations between the two mass functions is essentially impossible – however, we can attempt to address the *shape* of the mass function in this boundary region. That is try to answer the question “Does the star formation mass function turn over between 40 and $5 M_{\text{JUP}}$?” If it does, then we must determine where it does, as this is critical information needed to refine models of the star formation process.

Unfortunately, while sky surveys have been extremely successful at detecting field brown dwarfs, their unknown ages make the measurement of masses problematic. Such studies need to target stellar clusters of known age in order to estimate masses. Unfortunately, clusters close enough to the Sun for brown dwarfs to be detectable are large on the sky (typically 0.2–10 sq.deg.), and typically show low contrast against the low latitude background of field stars. Moreover, the photospheres of cool brown dwarfs are phenomenally complex, leading to real difficulties for theoretical models. This makes traditional colour-magnitude diagrams a poor means of selecting cluster members, because uncertainties force the selection of very large samples in colour-magnitude space, with poor hit-rates for *actual* cluster members. The resultant imaging samples then require substantial spectroscopic winnowing on 8–10m telescopes.

T dwarf methane absorption, however, is so spectrally unique, that it provides a potentially powerful tool for selecting candidate T dwarfs in clusters. Tinney et al. (2003) have looked at the absolute magnitudes at which methane may begin to appear in some representative clusters, and concluded that in nearby ($d \approx 150$ pc), 10–20 Myr old clusters like IC 2391 or IC 2602, the absolute magnitude for CH_4 to become detectable by methane imaging (equivalent to spectral types T2 and later) will be $M_H \sim 12.5$, or equivalently $H \sim 18.2$. Later T types will appear at at fainter magnitudes, with the more easily detectable levels of methane absorption seen in T5 dwarfs appearing around 1.5 mag fainter.

Using the available T dwarf models (see Tinney et al. 2003 and references therein), we can estimate the second-order *differential* corrections to this first-order methane onset estimate. If we adopt the absolute magnitude corresponding to an easily detectable spectral type of T5 as our measure (hereafter $M_{\text{CH}_4}^{\text{T5}}$), we can estimate offsets from the $M_{\text{CH}_4}^{\text{T5}} \approx 14$ of field

dwarfs to the $M_{\text{CH}_4}^{\text{T5}}$ for younger clusters, as well as the masses to which these $M_{\text{CH}_4}^{\text{T5}}$ values correspond. For clusters of age 100, 50, 10 & 5 Myr the relevant offsets are found to be (respectively) $\Delta M_{\text{CH}_4}^{\text{T5}} = -0.7, -1.0, -1.3$ & -1.5 and the masses to which these $M_{\text{CH}_4}^{\text{T5}}$ correspond are 0.02, 0.012, 0.008 & $0.006 M_{\odot}$. For any given cluster, therefore, a survey can be designed using CH_4 selection to probe mass functions at unprecedentedly low masses. As an example, the IRIS2 imager is able to detect T5 dwarfs in the IC 2391 cluster ($d=140$ pc, $\text{age}=20 \pm 10$ Myr) after just 8 hours of integration (i.e. 4 hours in each bandpass), reaching to a depth of $H=21$ over an area of 64 sq.arcmin., corresponding to a detection threshold mass of $\approx 10 M_{\text{JUP}}$.

The resulting T dwarf imaging candidates will still need to be followed up spectroscopically, in order to distinguish young cluster members, from old field T dwarf contaminants. But it is nonetheless true that contamination by *non-T dwarfs* can be arranged to be small, or negligible, vastly improving the speed of confirmation, or rejection, of cluster membership for T dwarfs.

4.2.3. Cool companions to Known Brown Dwarfs

Very rare astronomical objects (like T and Y dwarfs) are typically searched for by surveying very large chunks of the sky. An alternate approach is to rely on the fact that most astronomical objects are clustered, and so to search for rare objects in the vicinity of a objects of a similar nature. It was exactly such a search technique that revealed the first T dwarf Gl 229B (Nakajima et al. 1995). The invariable difficulty in such searches is telling the difference between a potentially interesting companion to the target in question, and the vast majority of background objects. In the case of Gl 229B, the companion was revealed by its common proper motion. Methane imaging offers a potentially powerful way to identify cool companions to nearby stars and brown dwarfs, without the need to wait for the year or more needed to confirm or deny common proper motion. For example, a few hours integration with the methane filters in IRIS2 can easily reach to sensitivities adequate to detect methane absorption in objects 3–4 magnitudes fainter than all the T dwarfs so far identified from 2MASS, making this a potentially easier way in which to find Y dwarfs than a large blind survey.

4.2.4. Methane Variability and “Weather”

There is now considerable evidence to indicate that many, if not most, brown dwarfs rotate quite rapidly, with either measured (Bailer-Jones & Lamm 2003; Clarke et al. 2002a,b; Enoch et al. 2003; Gelino et al. 2002; Koen 2003; Bailer-Jones & Mundt 2001; Tinney & Tolley 1999) or inferred (Bailer-Jones 2004; Smith et al. 2003; Mohanty & Basri 2003; Reid et al. 2002; Tinney & Reid 1998) rotation timescales of 1–10 h. L and T type brown dwarfs are also well known to suffer greater or lesser degrees of condensate and/or cloud layer formation (see e.g. Ackerman & Marley 2001; Allard et al. 2001; Burrows & Sharp 1999). So brown dwarfs have the two ingredients required for the existence of complex rotationally driven weather patterns on their surface. Unfortunately, despite much intensive searching (see references above) detailed evidence for weather variations in brown dwarfs remains elusive.

However, as the source of the dominant absorption feature in the spectra of T dwarfs, searches for variability in CH_4 absorption (reflecting an uneven surface coverage at the optical depths where these absorptions are formed) could be

extremely powerful (Tinney 2000). Jupiter, for example, is known to show strong surface features in the infrared where gaps in its methane layers allow the hotter, lower regions of the photosphere to shine through (see for example the images of Jupiter in Gelino & Marley (2000)). The nearly differential nature of methane imaging should make possible significantly higher precisions (i.e. <0.01 mag) in programs targeting single objects in extended campaigns, than have been achieved in this program. In particular, bright T dwarfs can be targeted (or larger telescopes used) to improve photon-counting uncertainties, observation of a single object for variability makes the zero-point uncertainty associated with the selection of an ensemble of background objects moot, and use of the $\text{CH}_4\text{s}-\text{CH}_4\text{l}$ colour should obviate many of the second-order differential extinction effects discussed by Bailer-Jones & Lamm (2003).

5. CONCLUSION

We have shown that methane filters can be used to efficiently detect and characterise T dwarfs. We have provided a procedure for calibrating methane filter observations onto a $\text{CH}_4\text{s}, \text{CH}_4\text{l}$ photometric system using 2MASS photometry as a calibration system. Five new T dwarfs discovered as part of the 2MASS Wide Field T dwarf Search using this technique have been presented. Finally we have discussed potential further uses for these methane filters including: the winnowing of large survey datasets for T and Y dwarfs; the detection of very low-mass brown dwarfs (as low as $10M_{\text{JUP}}$) in nearby

star clusters; the detection of cooler companions to already known brown dwarfs; and, the detection of variability signatures due to rotating cloud structures in T dwarfs.

The authors wish to gratefully acknowledge the Joint Astronomy Centre, Hawaii, for making their ORAC-DR code available, and for assisting the AAO in implementing it for IRIS2. This wonderful data reduction package has *significantly* improved the efficiency with which this observing program was carried out. We would also like to acknowledge Michael Richmond, Emmanuel Bertin and Tim Pearson – the authors of the `match`, `sextractor` and `PGPLOT` codes which contributed significantly to this work. AJB acknowledges support by the National Aeronautics and Space Administration (NASA) through the SIRTFF Fellowship program. JDK acknowledges the support of the Jet Propulsion Laboratory, California Institute of Technology, which is operated under contract with NASA. CGT joins his US colleagues in thanking his employer for paying him. This publication makes use of data from the Two Micron All Sky Survey, which is a joint project of the University of Massachusetts and the Infrared Processing and Analysis Center, funded by NASA and the NSF. It also makes use of the NASA/IPAC Infrared Science Archive, which is operated by the Jet Propulsion Laboratory, California Institute of Technology, under contract with the National Aeronautics and Space Administration.

REFERENCES

- Ackerman, A. S. & Marley, M. S. 2001, *ApJ*, 556, 872
 Allard, F., Hauschildt, P. H., Alexander, D. R., Tamani, A., & Schweitzer, A. 2001, *ApJ*, 556, 357
 Bailer-Jones, C. A. L. 2004, *A&A*, 419, 703
 Bailer-Jones C. A. L. & Lamm M. 2003, *MNRAS*, 339, 477
 Bailer-Jones C. A. L. & Mundt R. 2001, *A&A*, 367, 218
 Bertin, E. & Arnouts, S. *A&AS*, 117, 393
 Bessell, M. S. & Brett, J. M. 1988, *PASP*, 100, 1134
 Boss, A. P. 1988, *ApJ*, 331, 370
 Boss, A. P. 1993, in *The Realm of Interacting Binary Stars*, ed. Sahade et al. (Dordrecht: Kluwer), 355
 Boss, A. P. 2001, *ApJ*, 551, L167
 Bouvier, J., Moraux, E., Stauffer, J. R., Barrado y Navascués, D., & Cuillandre, J.-C. 2003, in *IAU Symp. 211, Brown Dwarfs* ed. E. L. Martín (San Francisco: ASP), 147
 Burgasser, A. J., Geballe, T. R., Golimowski, D. A., Leggett, S. K., Kirkpatrick, J. D., Knapp, G. R., & Fan, X. 2003a, in *IAU Symp. 211, Brown Dwarfs* ed. E. L. Martín (San Francisco: ASP), 377
 Burgasser, A. J., Kirkpatrick, J. D., McElwain, M. W., Cutri, R. M., Burgasser, A. J., & Strutskie, M. F. 2003b, *AJ*, 125, 850
 Burgasser, A. J., McElwain, M. W., & Kirkpatrick, J. D. 2003c, *AJ*, 126, 2487
 Burgasser, A. J., McElwain, M. W., Kirkpatrick, J. D., Cruz, K. L., Tinney, C. G., & Reid, I. N. 2004a, *AJ*, 127, 2856
 Burgasser, A. J., Tinney, C. G., Saumon, D., Marley, M. S., & Kirkpatrick, J. D. 2004b, *ApJ*, submitted
 Burgasser, A. J., et al. 2002b, *ApJ*, 564, 421
 Burgasser, A. J., Geballe, T. R., Leggett, S. K., Kirkpatrick, J. D., Golimowski, D. A., & Fan, X. 2005, *ApJ*, submitted
 Burrows, A. & Sharp, C. M. 1999, *ApJ*, 512, 843
 Clarke F. J., Tinney C. G., & Covey K. R. 2002a, *MNRAS*, 332, 361
 Clarke F. J., Oppenheimer B. R., & Tinney C. G. 2002b, *MNRAS*, 335, 1158
 Cutri, R. M. et al. 2003, *Explanatory Supplement to the 2MASS All Sky Data Release* (Pasadena: Caltech)
 Delfosse, X., Tinney, C. G., Forveille, T., Epchtein, N., Borsenberger, J., Fouque, P., & Kimeswenger, S. 1999 *A&AS*, 135, 41
 Delfosse, X., et al. 1997, *A&A*, 327, L25
 Enoch M. L., Brown M. E. & Burgasser A. J. 2003, *AJ*, 126, 1006
 Geballe, T. R. et al. 2002, *ApJ*, 564, 466
 Gelino C. R. & Marley M. S. 2000, in *ASP Conf. Ser. 212, From Giant Planets to Cool Stars*, ed. C. A. Griffith & M. S. Marley (San Francisco:ASP), 322
 Gelino C. R., Marley M. S., Holtzman J. A., Ackerman A. S., & Lodders K., 2002, *ApJ*, 577, 433
 Gizis, J. E. 2002, *ApJ*, 575, 484
 Golimowski, D. A., et al. 2004, *AJ*, 127, 3553
 Hambly, N. & The UKIDSS Consortium 2003, in *IAU Symp. 211, Brown Dwarfs* ed. E. L. Martín (San Francisco: ASP), 477
 Hawarden, T. G., Leggett, S. K., Letawsky, M. E., Ballantyne, D. R., & Casali, M. M. 2001, *MNRAS*, 325, 563.
 Herbst, T. M., Thompson, D., Fockenbrock, R., Rix, H.-W., & Beckwith, S. V. W. 1999, *ApJ*, 526, L17.
 Jones, H. R.A., Longmore, A. J., Allard, F., & Hauschildt, P. H. 1996, *MNRAS*, 280, 77
 Jones, H. R.A., Longmore, A. J., Jameson, R. F., & Mountain, C. M. 1994, *MNRAS*, 267, 413
 Kirkpatrick, J. D., et al. 2000, *AJ*, 120, 447
 Knapp, G.R et al. 2004, *AJ*, 127, 3553
 Koen C. 2003, *MNRAS*, 346, 473
 Krist, J. E., Golimowski, D. A., Schroeder, D. J., & Henry, T. J. 1998, *PASP*, 110, 1046
 Leggett, S. K., Allard, F., Geballe, T. R., Hauschildt, P. H., & Schweitzer, A. 2001, *ApJ*, 548, L908
 Leggett, S. K., the WFCAM Team, and the UKIDSS Cool Dwarf Group 2005, in press, *Proc. of the 13th Cool Stars Workshop*, ed. Favata, F. et al.
 Leggett, S. K., et al. 2002, *ApJ*, 564, 452
 Low, C. & Lynden-Bell, D. 1976, *MNRAS*, 176, 367
 Mainzer, A. K. & McLean, I. S. 2003, *ApJ*, 597, 555
 Mainzer, A. K., McLean, I. S., Sievers, J. L., & Young, E. T. 2004, *ApJ*, 604, 832
 Marcy, G., Butler, R. P., Vogt, S. S., & Fischer, D. A. 2004, in *IAU Symp. 213, Bioastronomy 2002: Life among the stars* ed. R. P. Norris & F. H. Stootman (San Francisco: ASP), 11
 McCook G. P. & Sion E. M. 1999, *ApJS*, 121, 1
 Mohanty, S. & Basri, G. 2003, *ApJ*, 583, 451
 Nakajima, T., Oppenheimer, B. R., Kulkarni, S. R., Golimowski, D. A., Matthews, K., & Durrance, S. T. 1995, *Nature*, 378, 463
 Reid, I. N., Burgasser, A. J., Cruz, K. L., Kirkpatrick, J. D., & Gizis, J. E. 2001, *AJ*, 1710
 Reid, I. N., Kirkpatrick, J. D., Liebert, J., Gizis, J. E., Dahn, C. C., & Monet, D. G. 2002 *AJ*, 124, 519
 Reipurth, B. & Clarke, C. 2001, *AJ*, 122, 432
 Rosenthal, E. D., Gurwell, M. A., & Ho, P. T. P. 1996, *Nature*, 384, 243

- Skrutskie, M. F. et al. 1997, in *The Impact of Large-Scale Near-IR Sky Surveys*, ed. F. Garzon (Dordrecht:Kluwer), 25
- Smith, V. V. et al. 2003, *ApJ*, 599, L107
- Stephens, D.C & Leggett, S. K. 2004, *PASP*, 116, 9
- Testi, L., Natta, A., Sheperd, D. S., & Wilner, D. J. 2001, *ApJ*, 554, L1087
- Tinney, C. G., Delfosse, X., Forveille, T., & Allard, F. 1998, *A&A*, 338, 1066
- Tinney, C. G. & Reid, I. N. 1998, *MNRAS*, 304, 119
- Tinney, C. G. 2000, in *ASP Conf. Ser. 212, From Giant Planets to Cool Stars*, ed. C. A. Griffith & M. S. Marley (San Francisco:ASP), 322-278
- Tinney C. G. & Tolley A. J. 1999, *MNRAS*, 304, 119
- Tinney, C. G., Burgasser, A., Kirkpatrick, J. D., & Reid, I. N. 2003 *AJ*, 126, 975
- Tokunaga, A. T., Simons, D. A., & Vacca, W. D. 2002, *PASP*, 114, 180

TABLE 7
CH₄S-CH₄L AND JHK PHOTOMETRY FOR A TO T DWARFS

Object Name		SpT	<i>n</i> ^a	J-H _{MKO} ^b	H-K _{MKO} ^b	J-K _{MKO} ^b	CH ₄ s-CH ₄ l ^c	CH ₄ s-CH ₄ l _{Diff} ^d	Src SpT ^e	Src JHK ^f
UKIRT FS										
FS10	GD50	DA	-1	-0.05	-0.14	-0.19	-0.09±0.06 (1)	-0.11±0.04 (1)	0	1
FS20	EG76	DA	-1	-0.01	-0.05	-0.07	-0.04±0.05 (1)	-0.06±0.02 (1)	0	1
FS34	EG141	DA	-1	-0.04	-0.09	-0.12	0.00±0.03 (2)	-0.02±0.01 (2)	0	1
FS7	SA94-242	A2	2	0.12	0.01	0.13	0.01±0.02 (3)	+0.06±0.02 (3)	1	1
FS11	SA96-83	A3	3	0.07	0.03	0.09	-0.01±0.02 (3)	+0.04±0.01 (3)	1	1
FS2	SA92-342	F5	15	0.19	0.03	0.22	-0.01±0.03 (1)	-0.03±0.01 (1)	1	1
FS4	SA93-317	F5	15	0.23	0.03	0.27	-0.01±0.03 (1)	+0.01±0.01 (1)	1	1
FS18	SA100-280	F8	18	0.24	0.05	0.29	0.02±0.02 (2)	+0.07±0.01 (2)	1	1
FS137		G1	21	0.25	0.05	0.30	0.03±0.02 (1)	+0.02±0.01 (2)	1	1
FS16		G1	21	0.29	0.06	0.34	0.06±0.01 (1)	+0.03±0.01 (1)	1	1
FS13	SA97-249	G4	24	0.31	0.05	0.36	0.00±0.01 (3)	+0.04±0.01 (3)	1	1
FS135		G5	25	0.30	0.06	0.35	0.03±0.01 (1)	+0.06±0.01 (1)	1	1
FS136		K2	31	0.52	0.12	0.64	0.11±0.01 (1)	+0.09±0.02 (1)	1	1
FS124	LHS254	M5	40	0.40	0.34	0.74	0.13±0.03 (1)	+0.18±0.01 (1)	2	1
FS128		M5	40	0.55	0.38	0.93	0.14±0.02 (1)	+0.16±0.01 (1)	2	1
FS129	LHS2397a	M8(+L7)	43	0.63	0.54	1.17	0.16±0.01 (4)	+0.21±0.01 (4)	2	1
L dwarfs										
2M1045-0149	2MASS J10452400-0149576	L1	46	0.65	0.63	1.27	0.18±0.03 (1)	+0.17±0.01 (1)	7	3
Kelu-1	2MASS J13054019-2541059	L2	47	0.78	0.67	1.45	0.20±0.02 (1)	+0.23±0.02 (1)	3	2
DEN1058-1548	DENIS-P J1058.7-1548	L3	48	0.84	0.74	1.57	0.22±0.02 (1)	+0.23±0.02 (1)	3	2
DEN1539-0520	DENIS-P J153941.96-052042.4	L4	49	0.69	0.57	1.26	0.14±0.02 (1)	+0.08±0.16 (1)	4	3
DEN1228-1547	DENIS-P J1228.2-1547AB	L5	50	0.88	0.69	1.57	0.20±0.03 (1)	+0.23±0.02 (1)	3	2
2M1507-1627	2MASS J15074769-1627386	L5	50	0.75	0.67	1.42	0.16±0.02 (1)	+0.20±0.01 (1)	3	3
DEN0255-4700 ^g	DENIS-P J0255.0-4700	L8	53	0.83	0.74	1.57	0.12±0.03 (1)	+0.18±0.01 (1)	3	4
T dwarfs										
SD0423-0414	SDSSp J042348.57-041403.5	T0	54	0.79	0.55	1.34	0.08±0.03 (2)	+0.15±0.02 (4)	5	3
SD1207+0244	SDSSp J120747.17+024424.8	T0.5	54.5	0.75	0.47	1.22	-0.05±0.05 (1)	+0.05±0.03 (1)	5	3
SD1254-0122	SDSSp J125453.90-012247.4	T2	56	0.53	0.29	0.82	-0.03±0.06 (1)	+0.04±0.02 (1)	5	3
SD1021-0304	SDSSp J102109.69-030420.1	T3.5	57.5	0.47	0.15	0.62	-0.30±0.07 (1)	-0.11±0.04 (4)	5	3
SD0207+0000	SDSSp J020742.83+000056.2	T4	58	0.01	-0.03	0.04	-0.29±0.04 (1)	-0.37±0.10 (1)	5	3
2M0559-1404	2MASS J05591914-1404488	T4.5	58.5	-0.16	-0.07	-0.09	-0.43±0.03 (1)	-0.40±0.02 (3)	5	3
2M0516-0445	2MASS J05160945-0445499	T5.5	59.5	-0.06	0.16	0.10	-0.79±0.03 (1)	-0.70±0.02 (3)	6	4
SD1110+011	SDSSp J111010.01+011613.1	T5.5	59.5	-0.10	0.17	0.07	-0.69±0.20 (2)	-0.66±0.12 (2)	5	3
2M2356-1553	2MASS J23565477-1553111	T5.5	59.5	-0.22	-0.03	-0.25	-0.93±0.04 (1)	-0.71±0.05 (4)	5	3
2M0243-2453	2MASS J02431371-2453298	T6	60	-0.26	0.05	-0.21	-0.79±0.05 (1)	-0.77±0.02 (3)	5	3
2M2228-4310	2MASS J22282889-4310262	T6	60	-0.05	-0.03	-0.08	-0.89±0.03 (1)	-0.82±0.02 (1)	5	4
SD1346-0031	SDSSp J134646.45-003150.4	T6.5	60.5	-0.35	0.11	-0.24	-1.00±0.05 (1)	-0.87±0.08 (1)	5	3
2M1217-0311	2MASS J12171110-0311131	T7	61	-0.42	0.06	-0.36	-1.44±0.08 (1)	-1.42±0.08 (1)	5	3
GI570d	2MASS J14571496-2121477	T7.5	61.5	-0.46	-0.24	-0.70	-1.54±0.04 (1)	-1.38±0.05 (4)	5	3
2M0415-0935	2MASS J04151954-0935066	T8	62	-0.51	-0.38	-0.13	-1.69±0.34 (1)	-1.66±0.05 (3)	5	3

^a *n* is the spectral subtype plus a constant for A-T dwarfs: 0 for an A dwarf; 10 for F; 20 for G; 29 for K; 35 for M; 45 for L and 54 for T. *n* is set to the placeholder value of -1 for white dwarfs.

^b J-H, H-K and J-K on the MKO photometric system. Typical uncertainties are <0.01 mag for UKIRT FS standards and <0.05 mag for the remaining objects.

^c The number of observations averaged to provide the quoted result are indicated in parentheses.

^d See text Section 2.5 for definition of CH₄s-CH₄l_{Diff}. The number of observations averaged to provide the quoted result are indicated in parentheses.

^e 0 - McCook & Sion (1999); 1 - Hawarden et al. (2001); 2 - Leggett et al. (2002); 3 - Kirkpatrick et al. (2000); 4 - Spectral type provided by D.Kirkpatrick (private communication) and determined using optical spectroscopy to estimate spectral types on the Kirkpatrick et al. (2000) system; 5 - Burgasser et al. (2005); 6 - Burgasser et al. (2003c); 7 - Gizis (2002)

^f 1 - UKIRT MKO photometric standards (see Section 2.3); 2 - Leggett et al. (2002); 3 - Knapp et al. (2004); 4 - converted 2MASS All Sky data into the MKO system using the conversion relations of Stephens & Leggett (2004)

^g The conversions from 2MASS to MKO photometry of Stephens & Leggett (2004) are essentially independent of spectral typing system for early-to-mid L dwarfs and T dwarfs, but are less so for late-type L dwarfs. In the case of DENIS-P J0255.0-4700 this could lead to an additional uncertainty in its MKO colours of <0.03 mag over and above the 0.05 mag relevant for the other L and T dwarfs so converted.

TABLE 8
CH₄S–CH₄L PHOTOMETRY, PROPER MOTIONS AND SPECTRAL TYPES FOR T DWARFS

Short Name	Full Name	SpT ^a	CH ₄ SpT ^b	CH ₄ S–CH ₄ L _{Diff} ^c	J–H _{2M} ^d	H–K _{S2M} ^d	J–K _{S2M} ^d	μ ^e	θ ^e	Src ^f
WFTS										
2M0034+0523	2MASS J00345157+0523050	T6.5	T6.5±0.3	−0.98±0.05 (1)	+0.09±0.09	−0.80±0.08	−0.71±0.04	0.8±0.3	85±15	1
2M0050-3322	2MASS J00501994-3322402	...	T7.1±0.3	−1.24±0.06 (1)	+0.09±0.20	+0.60±0.27	+0.69±0.20	1.5±0.1	53±5	3
2M0348-6022	2MASS J03480772-6022270	T7	T7.4±0.3	−1.37±0.06 (1)	−0.24±0.15	−0.04±0.27	−0.28±0.24	0.76±0.06	196±6	1
2M0939-2448	2MASS J09393548-2448279	...	T8.2±0.3	−1.80±0.14 (1)	+0.18±0.18	−0.76±0.15	−0.58±0.10	1.15±0.06	155±1	3
2M0949-1545	2MASS J09490860-1545485	...	T0.3±1.5	+0.03±0.03 (2)	+0.89±0.16	+0.04±0.20	+0.92±0.20	0.10±0.04	271±34	3
2M1114-2618	2MASS J11145133-2618235	...	T7.5±0.3	−1.40±0.07 (1)	+0.12±0.15	−0.38±0.12	−0.25±0.08	3.05±0.04	263.2±0.8	3
2M1122-3512	2MASS J11220826-3512363	...	T1.5±1.1	−0.06±0.02 (1)	+0.66±0.06	−0.02±0.08	+0.64±0.07	0.29±0.03	211±8	3
2M1231+0847	2MASS J12314753+0847331	T5.5	T5.5±0.4	−0.68±0.04 (1)	+0.26±0.13	+0.09±0.22	+0.35±0.21	1.61±0.07	227±4	1
2M1828-4849	2MASS J18283572-4849046	T5.5	T5.0±0.5	−0.57±0.03 (1)	+0.27±0.09	−0.27±0.16	−0.01±0.15	0.34±0.06	84±10	1
2M2331-4718	2MASS J23312378-4718274	T5	T4.7±0.5	−0.51±0.03 (1)	+0.15±0.16	+0.12±0.25	+0.27±0.21	0.20±0.07	118±6	1
Other										
SD0151+1244	SDSSp J015141.69+124429.6	T1	L5–T0	+0.18±0.04 (2)	+0.96±0.17	+0.42±0.22	+1.38±0.23	0.90±0.05	100±2	1
SD0207+0000	SDSSp J020742.83+000056.2	T4	T4.0±0.8	−0.37±0.10 (1)	+0.40±0.15	...	+1.39±0.15	0.30±0.13	101±13	1
2M0243-2453	2MASS J02431371-2453298	T6	T5.8±0.5	−0.77±0.02 (3)	+0.24±0.12	−0.08±0.20	+0.17±0.17	0.28±0.05	229±25	1
2M0415-0935	2MASS J04151954-0935066	T8	T8.0±0.2	−1.66±0.03 (3)	+0.16±0.13	+0.11±0.23	+0.27±0.21	2.31±0.04	76±1	1
SD0423-0414	SDSSp J042348.57-041403.5	T0	L3–T0	+0.15±0.02 (4)	+1.00±0.04	+0.53±0.05	+1.54±0.04	0.29±0.04	281±9	1
2M0516-0445	2MASS J05160945-0445499	T5.5	T5.6±0.3	−0.70±0.02 (3)	+0.26±0.18	+0.23±0.26	+0.50±0.22	0.30±0.04	234±9	2
2M0559-1404	2MASS J05591914-1404488	T4.5	T4.1±0.4	−0.40±0.02 (3)	+0.12±0.05	+0.10±0.07	+0.22±0.06	0.72±0.04	120±1	1
SD1021-0304	SDSSp J102109.69-030420.1	T3.5	T2.3±1.0	−0.11±0.04 (4)	+0.91±0.14	+0.22±0.20	+1.13±0.19	0.17±0.04	252±40	1
SD1110+0116	SDSSp J111010.01+011613.1	T5.5	T5.5±0.5	−0.66±0.12 (2)	+0.42±0.18	+0.79±0.14	+1.21±0.12	0.34±0.10	110±27	1
SD1207+0244	SDSSp J120747.17+024424.8	T0.5	T0±1.5	+0.05±0.03 (1)	+1.02±0.09	+0.57±0.09	+1.59±0.09	0.39±0.09	286±13	1
2M1217-0311	2MASS J12171110-0311131	T7	T7.5±0.3	−1.42±0.08 (1)	+0.11±0.13	−0.14±0.12	−0.03±0.06	1.00±0.06	278±3	1
2M1225-2739	2MASS J12255432-2739476AB	T6	T6.4±0.3	−0.89±0.06 (2)	+0.16±0.09	+0.03±0.17	+0.19±0.15	0.72±0.03	146±1	1
SD1254-0122	SDSSp J125453.90-012247.4	T2	T0.1±1.5	+0.04±0.02 (1)	+0.80±0.04	+0.25±0.06	+1.05±0.06	0.45±0.06	285±6	1
SD1346-0031	SDSSp J134646.45-003150.4	T6.5	T5.8±0.4	−0.87±0.08 (1)	+0.54±0.16	−0.31±0.30	+0.23±0.29	< 0.24	...	1
Gl570d		T7.5	T7.5±0.2	−1.38±0.05 (4)	+0.06±0.10	+0.03±0.18	+0.08±0.16	1.99±0.03	147.7±0.6	1
2M1534-2952	2MASS J15344984-2952274AB	...	T4.4±0.5	−0.45±0.01 (1)	+0.03±0.11	+0.02±0.15	+0.06±0.13	0.28±0.03	156±3	1
2M1546-3325	2MASS J15462718-3325111	...	T5.1±0.4	−0.59±0.01 (1)	+0.19±0.10	−0.04±0.20	+0.15±0.19	0.25±0.04	38±12	1
SD1624+0029	SDSSp J162414.37+002915.6	T6	T5.9±0.4	−0.79±0.03 (1)	−0.03±0.11	+0.01±0.10	−0.02±0.05	0.34±0.07	256±18	1
SD1750+1759	SDSSp J175032.96+175903.9	T3	T2.6±0.9	−0.18±0.04 (1)	+0.39±0.16	+0.47±0.23	+0.86±0.21	0.22±0.08	100±12	1
ϵ Ind BC		...	T1.7±1.0	−0.09±0.01 (3)	+0.60±0.03	+0.10±0.03	+0.70±0.03	4.74±0.02	120.6±0.2	1
2M2228-4310	2MASS J22282889-4310262	T6	T6.0±0.4	−0.82±0.02 (1)	+0.30±0.14	+0.07±0.24	+0.37±0.22	0.35±0.05	164±5	1
2M2339+1352	2MASS J23391025+1352284	T5	T4.6±0.4	−0.47±0.03 (2)	+0.42±0.19	−0.32±0.34	+0.09±0.33	1.12±0.20	156±4	1
2M2356-1553	2MASS J23565477-1553111	T5.5	T5.7±0.3	−0.71±0.04 (4)	+0.19±0.11	−0.14±0.21	+0.05±0.19	0.77±0.04	211±7	1

^a Spectroscopic spectral type.

^b Methane spectral type, derived from CH₄S–CH₄L_{Diff} and equation 2.

^c See Section 2.5 for definition of CH₄S–CH₄L_{Diff}. The number of observations averaged to produce the measurement listed are indicated in parentheses.

^d J–H, H–Ks and J–Ks on the 2MASS photometric system. ‘.’ indicates object was not detected in the 2MASS Ks band, and 95% confidence upper limit has been used to derive the colour, the quoted uncertainty of which is due only to the J detection. SD0207+0000 was not detected in H or Ks by 2MASS.

^e Proper motion magnitude (μ in $''$ /yr) and direction (θ in degrees east of north). Many of the T dwarfs listed in Table 8 will be at distances of 7–20 pc, and will have annual parallax motions of 0.125–0.05 $''$, which we have not attempted to control. These will introduce proper motion uncertainties of a magnitude similar to those due to the precision of the astrometric transformation between the two epochs

^f Source for spectroscopic spectral type. 1 - Burgasser et al. (2005). 2 - spectra from Leggett et al. (2002); Knapp et al. (2004); Burgasser et al. (2003b,c, 2004a) classified using procedure described in Section 3.2. 3 - IRIS2 spectral types as described in Section 3.2. If no spectral type listed for a T dwarf then no “hybrid” spectral type has been published, or could be calculated from available archival data.